



*Annual Review of Marine Science*

# The Water Mass Transformation Framework for Ocean Physics and Biogeochemistry

Sjoerd Groeskamp,<sup>1</sup> Stephen M. Griffies,<sup>2,3</sup>  
Daniele Iudicone,<sup>4</sup> Robert Marsh,<sup>5</sup>  
A.J. George Nurser,<sup>5</sup> and Jan D. Zika<sup>1</sup>

<sup>1</sup>School of Mathematics and Statistics, University of New South Wales, Sydney, New South Wales 2052, Australia; email: s.groeskamp@unsw.edu.au

<sup>2</sup>Geophysical Fluid Dynamics Laboratory, National Oceanic and Atmospheric Administration, Princeton, New Jersey 08540, USA

<sup>3</sup>Program in Atmospheric and Oceanic Sciences, Princeton University, Princeton, New Jersey 08540, USA

<sup>4</sup>Laboratory of Ecology and Evolution of Plankton, Stazione Zoologica Anton Dohrn, 80121 Naples, Italy; email: iudicone@szn.it

<sup>5</sup>National Oceanography Centre, Southampton SO14 3ZH, United Kingdom

Annu. Rev. Mar. Sci. 2019. 11:21.1–21.35

The *Annual Review of Marine Science* is online at  
[marine.annualreviews.org](http://marine.annualreviews.org)

<https://doi.org/10.1146/annurev-marine-010318-095421>

Copyright © 2019 by Annual Reviews.  
All rights reserved

## Keywords

water mass transformation, biogeochemistry, tracers, circulation, ventilation, subduction, mixing, air-sea fluxes, diagnostics, AMOC

## Abstract

The water mass transformation (WMT) framework weaves together circulation, thermodynamics, and biogeochemistry into a description of the ocean that complements traditional Eulerian and Lagrangian methods. In so doing, a WMT analysis renders novel insights and predictive capabilities for studies of ocean physics and biogeochemistry. In this review, we describe fundamentals of the WMT framework and illustrate its practical analysis capabilities. We show how it provides a robust methodology to characterize and quantify the impact of physical processes on buoyancy and other thermodynamic fields. We also detail how to extend WMT to insightful analysis of biogeochemical cycles.

21.1



Review in Advance first posted on  
September 19, 2018. (Changes may  
still occur before final publication.)

**Water mass transformation (WMT):** the mass transport of seawater through a surface with a constant property value

**Fluid element:** a tiny fluid region of constant mass moving with the flow whose tracer content changes via diffusion or biogeochemistry

## 1. INTRODUCTION

In 1750, Captain Henry Ellis lowered a bucket into the subtropical Atlantic and discovered that seawater at depth is relatively cold (Ellis 1751, Richardson 2008). Rumford [1968 (1798)] hypothesized that this water is cold because it moves equatorward at depth from its colder, high-latitude origin. In doing so, Rumford was one of the first oceanographers to use a tracer—in this case, temperature—to define a water mass, trace it back to its origin, and infer a circulation (without a single measurement of the circulation itself) (**Figure 1a**).

In the following centuries, oceanographers expanded their definitions of water masses to include other tracers, such as salinity and oxygen. A key feature of this analysis is the development of an understanding of how water masses are both transported by the circulation and modified, or transformed, through processes such as mixing and biogeochemical activity. The understanding of such processes, combined with observational estimates of water mass transformation (WMT), led to the construction of a global conveyor belt circulation (Broecker 1982), thus providing an important step toward understanding the globally interconnected ocean circulation.

There are relatively few direct measurements of dynamical ocean fields such as currents on a scale sufficient to quantify the global ocean circulation. Consequently, oceanographers seek indirect methods to gain a conceptual and quantitative understanding of ocean circulation. WMT analysis offers one such method.

In this review, we describe how a WMT framework can be used to understand both physical and biogeochemical processes and the associated circulation. Part of our motivation is to enhance the appreciation among physicists and biogeochemists that WMT provides a natural way to think about ocean tracer circulation and storage and reveals a mechanistic and predictive understanding of the ocean. We aim to provide sufficient conceptual, mathematical, and practical details for the reader to be able to implement and interpret a WMT analysis using observational or model data.

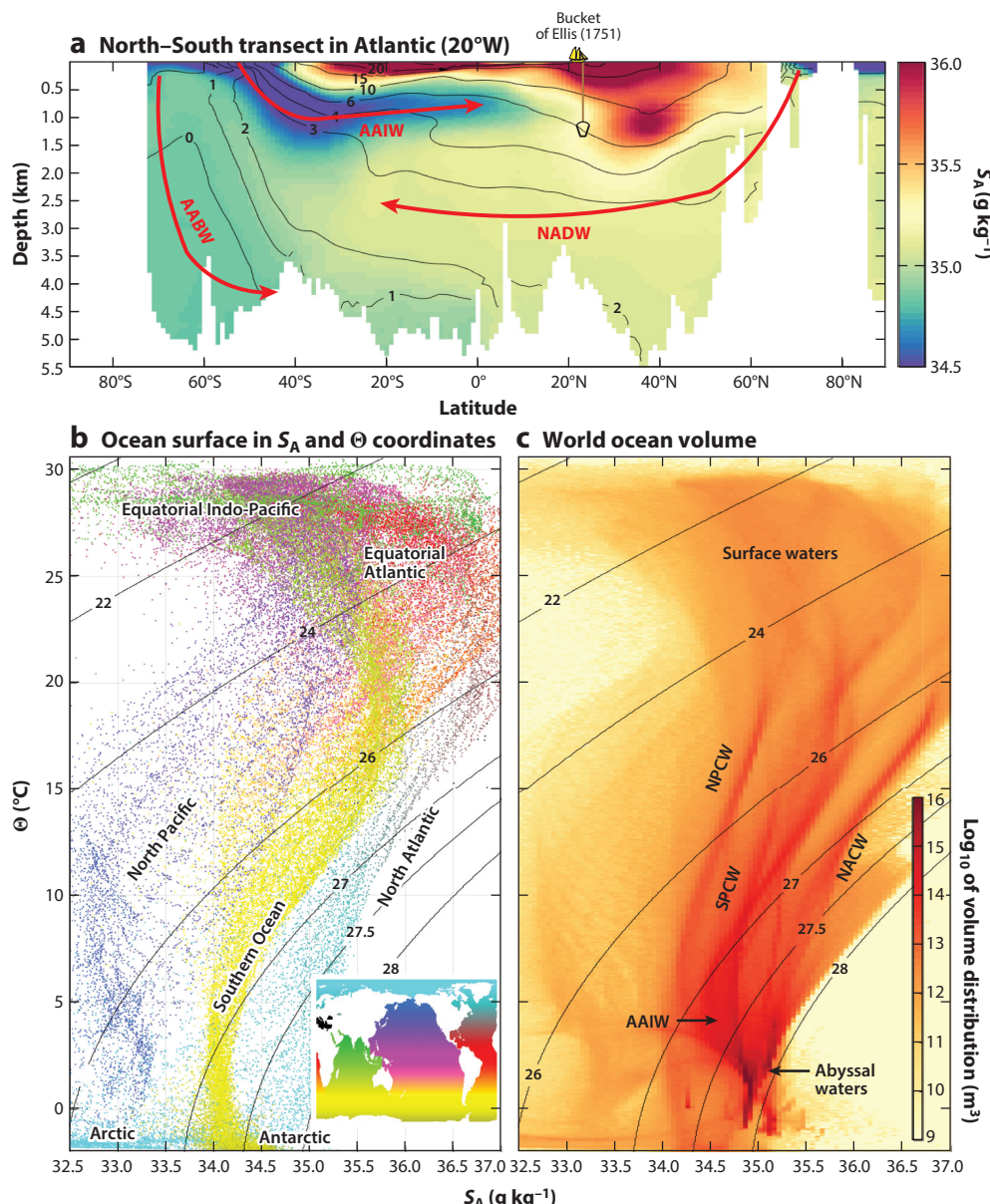
### 1.1. Viewing the Ocean According to Water Masses

We define water masses to be bulk regions of the ocean fluid characterized by scalar properties such as salinity ( $S$ ) and Conservative Temperature ( $\Theta$ ) and biogeochemical properties such as dissolved concentrations of carbon, oxygen, or nutrients.<sup>1</sup> Water masses provide a coarse-grained discretization or partitioning of the ocean into conceptually distinct pieces whose origin, evolution, and fate can be measured, studied, and modeled (**Figure 1**). This approach allows for measures of ocean circulation within the WMT phase space even without directly measuring the circulation, thus providing a view of the world ocean through the lens afforded by scalar properties rather than traditional Eulerian geographical coordinates (Defant 1936, Wüst 1936, Sverdrup et al. 1942) (see the sidebar titled Water Mass Transformation Phase Space as a Complement to Eulerian and Lagrangian Descriptions).

### 1.2. Processes Causing Water Mass Transformation

A fluid element (Olbers et al. 2012, p. 3) is exposed to various processes, including property exchanges with the atmosphere (air-sea fluxes) or adjacent seawater elements (mixing). These processes are the root cause for the transformation of water masses. Walin (1977, 1982) developed

<sup>1</sup> $S$  refers to a generic salinity, which is Absolute Salinity ( $S_A$ ) (McDougall et al. 2012) for observation-based applications. Conservative Temperature ( $\Theta$ ) is proportional to potential enthalpy and provides a measure of ocean heat content (McDougall 2003, Graham & McDougall 2013).

**Figure 1**

Defining water masses based on their Absolute Salinity ( $S_A$ ) and Conservative Temperature ( $\Theta$ ) properties. (a) A transect of  $S_A$  (color) with  $\Theta$  contours superimposed, using data from *World Ocean Database 2013* (Boyer et al. 2013), including the position of the bucket of Ellis (1751). Classical water masses are defined based on their  $S_A$  and  $\Theta$ . For example, Antarctic Intermediate Water (AAIW) is defined by its low  $S_A$ , Antarctic Bottom Water (AABW) is the densest water in the world ocean, and North Atlantic Deep Water (NADW) has origins in the north and sits above AABW. The red arrows indicate examples of inferred circulation based on the origin and fate of the water masses. (b) The geographical locations of the surface ocean in  $S_A$  and  $\Theta$  coordinates, according to the color coding of the inset (Zika et al. 2012). (c) The volume of the world ocean in  $S_A$  and  $\Theta$  coordinates (Worthington 1981). North Atlantic Central Water (NACW), North Pacific Central Water (NPCW), South Pacific Central Water (SPCW), and AAIW are visible as branches of high volume concentration, reaching out to higher temperatures at relatively constant salinity.

## WATER MASS TRANSFORMATION PHASE SPACE AS A COMPLEMENT TO EULERIAN AND LAGRANGIAN DESCRIPTIONS

The WMT framework formulates mass budgets for seawater bounded by smooth scalar surfaces and relates ocean circulation to processes leading to material changes in these surfaces. The WMT phase space is the configuration space for this circulation. Surfaces defining the WMT phase space generally do not have a one-to-one relation to geographical space, because the surfaces can be nonmonotonic in nature (see **Figure 3** in Section 2) or even disconnected. Consequently, the WMT phase space is not suitable for describing forces between spatially local fluid elements (i.e., contact forces such as pressure and frictional stress), so it is not a suitable kinematic framework to formulate Newton's laws of motion. Instead, the WMT phase space offers a powerful complement to Eulerian and Lagrangian perspectives, revealing novel insights into ocean circulation that are otherwise obscured. Indeed, for many questions of ocean climate and biogeochemistry, the WMT perspective is optimal for developing a mechanistic understanding of observations and numerical simulations.

a framework that marries aspects of Eulerian and Lagrangian kinematics, optimized to characterize and quantify the transformation of water masses due to such processes.

Most seawater properties experience strong changes near the surface and bottom boundaries, whereas interior property changes (e.g., mixing) are relatively weak. However, interior changes generally act over larger volumes and so make an important contribution to ocean property distributions. The WMT framework links transformation rates due to boundary-layer fluxes and mixing, offering the means to infer one from the other. That is, one can use the WMT framework to infer interior transformation from direct measurements of boundary-layer fluxes in models and observations, or to infer boundary-layer fluxes from direct measurements of interior transformation.

The WMT study by Walin (1982) focused on the heat budget for the North Atlantic, thus using temperature to mark water masses. Salinity is a key scalar property for WMT analysis when focusing on estuarine flow or the hydrological cycle (Walin 1977, Zika et al. 2015, Döös et al. 2016). Even so, the most common scalar property for a WMT analysis is buoyancy, or its approximation as provided by potential density (Speer & Tziperman 1992). As discussed in Section 1.3, buoyancy offers a direct connection to the ocean circulation.

### 1.3. Buoyancy Stratification and the Pancake Ocean

The following analogy illustrates the utility of buoyancy as a marker of water masses. Imagine a slightly tilted pile of Dutch pancakes sweetened with Canadian maple syrup. As the maple syrup is poured onto the top pancake, it readily spills over the sides but only slowly penetrates through to the interior. The disparate syrup transport arises because there is enhanced resistance to movement through a pancake but little resistance to movement along a pancake surface. We make use of this pancake analogy to conceptualize the stratification of ocean buoyancy and its influence on the associated transport of matter and heat.

Buoyancy measures the gravitational acceleration on a fluid element relative to the surrounding fluid. As a result, light seawater (high buoyancy) rises above heavy seawater (low buoyancy). Two fluid elements are neutrally buoyant when buoyancy does not force either element to move above or below the other. Though there are subtleties to be considered (McDougall et al. 2014), it is generally useful to conceive of the ocean away from boundary layers as a pile of neutrally buoyant



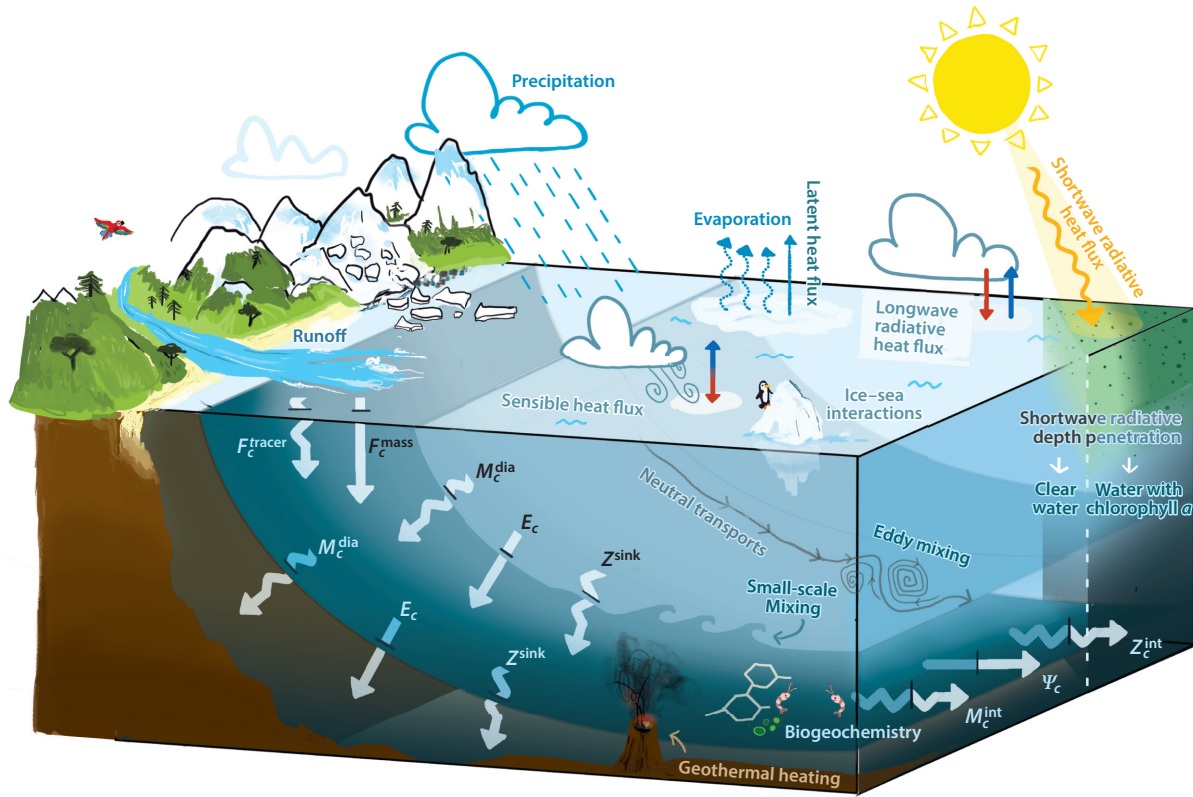
**Figure 2**

Illustration of processes that modify the ocean buoyancy or tracer concentration of a volume bounded by two neutral surfaces: the air-sea interface and an interior boundary. Red and blue surface arrows indicate heating and cooling, respectively. Changes in the tracer budget due to mass and tracer fluxes are indicated by straight and wavy white arrows, respectively, as specified in Equation 32 in Section 4.

surfaces (neutral surfaces, i.e., the pancakes), with fluid moving more readily along a neutral surface (epineutral transport) than through a neutral surface (dianeutral transport).

**1.3.1. Buoyancy changes in boundary layers and the interior.** Buoyancy sources in boundary layers arise from the direct transfer of heat, salt, and fresh water across the air-sea, ice-sea, and earth-sea boundaries. Such sources include turbulent and radiative heat fluxes, precipitation, evaporation, river runoff, sea-ice brine rejection, or geothermal heating along midocean rifts (Figure 2).

Boundary-layer forcing leads to the formation of water masses with a particular buoyancy characteristic that then subduct into the ocean interior, away from boundary layers. Once the water masses are in the ocean interior, changes in buoyancy arise mainly from mechanical or convective mixing of waters with different buoyancy. Mechanical mixing is generally of limited magnitude away from ocean boundaries, and convective mixing zones occupy a small fraction of the global ocean, so that interior buoyancy mixing is generally quite small. Consequently, once the buoyancy of a fluid element is set at the boundary, it generally retains that buoyancy within the ocean interior.

**Neutral surface ( $\gamma$ ):**  
a surface along which fluid elements can move without experiencing a buoyant restoring force

This phenomenology establishes a fundamental character of the ocean interior: Away from frictional or turbulent boundaries, interior motions transport and stir fluid elements along neutral surfaces. Stirring leads to the downscale transfer of tracer variance toward molecular mixing. This epineutral mixing is roughly  $10^7$ – $10^8$  times more efficient than dianeutral mixing. As a result, properties are relatively uniform along neutral surfaces. At least since Iselin (1939), observations of uniform properties along neutral surfaces have been used to infer the preferred direction of fluid transport along neutral directions. We are therefore led to conceive of ocean scalar transport as a superposition of (*a*) movement along neutral directions that extends from boundaries into the interior (epineutral transport) and (*b*) a much weaker dianeutral transport (Solomon 1971, McDougall & Church 1986, Griffies 2004, McDougall et al. 2014).

**1.3.2. Dianeutral transport and associated circulation.** Although typically smaller than epineutral transport, dianeutral transport remains critically important for ocean dynamics and biogeochemistry. First and foremost, it establishes the vertical buoyancy stratification that affects both the vertical transport of matter and heat and the characteristics of dynamical motions in a stratified ocean. In addition, because properties tend to have strong gradients in the dianeutral direction, a relatively small dianeutral transport can lead to a relatively large change in the property distribution and associated vertical stratification. The vertical extents of neutral surfaces that outcrop at the ocean surface—and associated epineutral transports—are limited to 2,000 m or shallower (Toggweiler & Samuels 1998, Sloyan & Rintoul 2001) for the majority of the ocean. As a result, below 2,000 m, the main mechanism by which properties can exchange with the deep ocean is by crossing neutral surfaces. As shown in this review, a buoyancy-based WMT analysis provides the means to conceptually and quantitatively characterize the dianeutral component of ocean circulation even without direct observations of that circulation.

#### 1.4. Content of this Review

In the remainder of this review, Section 2 provides a general framework that defines WMT and unifies different views found in the literature (Walsh 1982, Marshall et al. 1999, Nurser et al. 1999). In Section 3, the WMT framework is then specialized to the case of buoyancy to directly link with ocean circulation. In Section 4, we show how, with modest extension, the buoyancy-based WMT framework of Section 3 can be used to understand and quantify the distributions of properties dissolved in the fluid (e.g., carbon) and their connection to circulation and physical or biogeochemical processes. This merger allows for a unified analysis of tracer dynamics within buoyancy layers, thus distinctly quantifying the contribution of ocean circulation and tracer dynamics (diffusion and biogeochemical sources) on tracer budgets. In Section 5, we highlight areas of research where WMT thinking has proved useful, and in Section 6, we emphasize the growing importance of WMT thinking for addressing climate and ecosystem questions. The main text is then supported by four technical appendices (Sections 7–10).

## 2. FOUNDATIONS OF THE WATER MASS TRANSFORMATION FRAMEWORK

In this section, we classify seawater masses according to the value of an arbitrary scalar property  $\lambda$ . We define WMT as the mass transport of seawater through a surface of constant  $\lambda$ —that is, the area-integrated mass flux (density times velocity) from one  $\lambda$  layer to another. As WMT is a function of  $\lambda$ , the scalar property  $\lambda$  serves to define both surfaces in geographical space and the WMT phase space coordinate. We then introduce the notion of water mass formation (WMF),



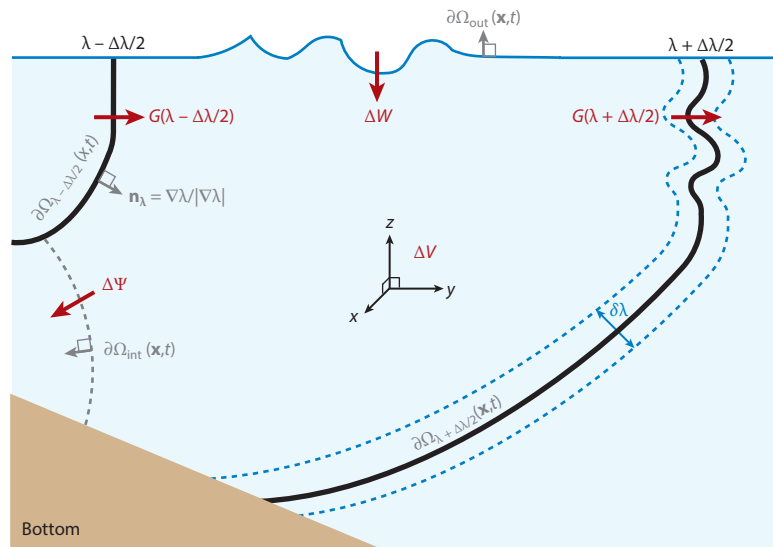


**Figure 3**

Illustration of water mass transformation  $G(\lambda)$  and water mass formation  $\Delta V$  for arbitrary control volumes. The domain encompassing the volume  $\Delta V$ , referred to as  $\Omega(\lambda)$  in the text, contains all the seawater within  $\lambda \pm \Delta\lambda/2$  and has a total mass of  $\Delta M$ . Here,  $\Delta V$  has open boundaries at the surface ( $\partial\Omega_{out}$ ) and interior ( $\partial\Omega_{int}$ ). Red arrows indicate mass transports due to the water mass transformation  $G$  (positive toward larger  $\lambda$ ), air-sea mass flux  $\Delta W$  (positive when entering the ocean), and mass flow out of the domain interior  $\Delta\Psi$  (residual mean flow, positive when leaving the region). The dashed blue lines of width  $\delta\lambda$  around the boundary  $\lambda - \Delta\lambda/2$  indicate a region over which  $G$  is numerically estimated [details explained in Appendix 1 (Section 7.5)]. Note the generally nonmonotonic nature of the  $\lambda$  iso-surfaces, here illustrated by vertical overturns on the  $\lambda + \Delta\lambda$  boundary. Such overturns and possible disconnected regions are handled by the water mass transformation formalism.

formulated as a seawater mass budget for regions defined by  $\lambda$  surfaces (Figure 3), which quantifies the creation or destruction of a particular water mass through the convergence of WMT plus added mass through boundaries.

We show that WMT can be expressed in terms of material (Lagrangian) time changes in the scalar property, equivalently written as  $\dot{\lambda} = D\lambda/Dt$ . For example, if  $\lambda = \Theta$ , then the WMT quantifies diathermal transport (Walsh 1982), and  $\dot{\Theta}$  results from (but is not limited to) irreversible mixing processes and air-sea heat fluxes. For a biogeochemical tracer such as oxygen ( $\lambda = O_2$ ), material changes may also result from biogeochemical sources and sinks. When  $\lambda = z$ , WMT quantifies the vertical transport across geopotential surfaces, and  $\dot{z} = w$  can arise from reversible processes (such as undulations of linear internal gravity waves) and irreversible processes (such as buoyancy mixing that leads to vertical motion). In Section 3, we quantify the dianeutral circulation by setting  $\lambda = \gamma$ , where  $\gamma$  is a neutrally buoyant surface (the pancake analogy). Finally, in Section 4.6, we use  $\lambda = -(z + b)$  as the depth measured with respect to the mixed-layer base  $b$  to define and quantify ventilation.

## 2.1. Defining Water Mass Transformation

Consider a surface along which a scalar property  $\lambda$  is constant. The unit normal vector to this surface is given by  $\hat{n}_\lambda = \nabla\lambda |\nabla\lambda|^{-1}$ , with our choice being to orient  $\hat{n}_\lambda$  in the direction of

**Water mass formation (WMF):**  
the creation or destruction of a water mass with a particular property



**Dia-surface velocity component ( $u^{\text{dia}}$ ):**  
the net volume flux through a surface per unit area ( $\text{m}^3 \text{ s}^{-1}/\text{m}^2 = \text{m s}^{-1}$ )

increasing  $\lambda$  (up the  $\lambda$  gradient; **Figure 3**). The unit normal is defined as long as  $|\nabla\lambda| \neq 0$ , which means that  $\lambda$  provides a family of surfaces that can partition the ocean fluid into distinct property classes.

Matter transport through a  $\lambda$  surface is determined by the dia-surface velocity component,  $u^{\text{dia}}$  ( $\text{m s}^{-1}$ ). As the  $\lambda$  surface is generally moving, we determine  $u^{\text{dia}}$  as the difference between (a) the velocity of a fluid element,  $\mathbf{u}$ , moving in the direction normal to the surface, and (b) the velocity of a point on the surface,  $\mathbf{u}_\lambda$ , moving in the direction normal to itself (e.g., figure 3 of Groeskamp et al. 2014a and section 6.7 of Griffies 2004), such that

$$u^{\text{dia}} \equiv \hat{\mathbf{n}}_\lambda \cdot (\mathbf{u} - \mathbf{u}_\lambda). \quad 1.$$

When both the fluid and the surface move in the same direction with the same speed,  $u^{\text{dia}}$  is 0, so there is no transport through the surface. By construction, positive values of  $u^{\text{dia}}$  denote water moving into regions of larger  $\lambda$ .

We measure the seawater mass transport,  $G(\lambda^*)$ , through a particular surface  $\lambda = \lambda^*$  by computing the area integral of  $\rho u^{\text{dia}}$  over the surface

$$G(\lambda^*) = \iint_{\lambda(\mathbf{x},t)=\lambda^*} \rho u^{\text{dia}} \, dA. \quad 2.$$

Here,  $dA$  is the area element on the  $\lambda = \lambda^*$  surface,  $\mathbf{x} = (x, y, z)$  represents coordinates in geographical space, and  $\rho$  is the in situ seawater density. Note that if we make the oceanic Boussinesq approximation, we replace  $\rho$  in Equation 2 with a constant density  $\rho_0$ , in which case it is common to focus on volume transport rather than mass transport.  $G(\lambda^*)$  is the WMT ( $\text{kg s}^{-1}$ ) that measures the mass per unit time of seawater crossing the surface  $\lambda = \lambda^*$ . This defining expression for  $G(\lambda^*)$  is valid even when the  $\lambda$  surface is discontinuous or nonmonotonic in any direction (**Figure 3**). The formalism does not require a one-to-one relation between  $\lambda$  iso-surfaces and geographical space  $(x, y, z)$ .

## 2.2. Water Mass Transformation Expressed as a Material Property Change

The temperature of a fluid element changes when crossing an isotherm. Analogously, a fluid element changes its  $\lambda$  value when there is WMT through a  $\lambda$  iso-surface. This basic point fundamentally connects the dia-surface volume flux crossing a  $\lambda$  surface ( $u^{\text{dia}}$ ) to material changes in  $\lambda$  ( $\dot{\lambda}$ ). This connection is key to formulating the equations of WMT. The mathematical relation  $u^{\text{dia}} = \dot{\lambda}/|\nabla\lambda|$  [Equation 39, derived in Appendix 1 (Section 7.1)] states that in the absence of material changes ( $\dot{\lambda} = 0$ ), i.e., for a material property surface, there is no dia-surface flux ( $u^{\text{dia}} = 0$ ) and thus no WMT [ $G(\lambda^*) = 0$ ]. Substituting into Equation 2 renders the WMT

$$G(\lambda^*) = \iint_{\lambda(\mathbf{x},t)=\lambda^*} \frac{\rho \dot{\lambda} \, dA}{|\nabla\lambda|}. \quad 3.$$

In summary, the presence of material time changes ( $\dot{\lambda} \neq 0$ ) leads to the movement of mass across  $\lambda$  surfaces, thus producing either an inflation or deflation of mass within a  $\lambda$  layer. Notably,  $u^{\text{dia}}$  is inversely proportional to  $\lambda$  gradients, so that regions of larger  $|\nabla\lambda|$  have relatively weaker transformation for a given  $\dot{\lambda}$ .

For many practical and conceptual purposes, it is useful to convert the surface integral represented by Equation 3 into the  $\lambda$  divergence of a volume integral:

$$G(\lambda) = \frac{\partial}{\partial \lambda} \iiint_{\lambda' \leq \lambda} \rho \dot{\lambda}' \, dV, \quad 4.$$

where the volume integral is computed over all values of  $\lambda'$  less than or equal to  $\lambda$ . This identity equates WMT to the nonzero divergence in  $\lambda$  space of the volume-integrated material changes. The mathematical identity represented by Equation 4 was first utilized by Marshall et al. (1999) and serves as the foundation for many applications of WMT. Further discussion of Equation 4, including its derivation using the fundamental theorem of calculus as well as its practical evaluation, is provided in Appendix 1 (Section 7).

### 2.3. Mass Budget and Water Mass Formation

We now derive the mass budget for a water mass bounded by two  $\lambda$  iso-surfaces. Specifically, we consider the geographical region (domain),  $\Omega(\lambda)$ , defined between iso-surfaces  $\lambda - \Delta\lambda/2$  and  $\lambda + \Delta\lambda/2$ . The volume ( $\Delta V$ ) and mass ( $\Delta M$ ) of this water mass are determined by

$$\Delta V(\lambda) = \iiint_{\Omega(\lambda)} dV, \quad \Delta M(\lambda) = \iiint_{\Omega(\lambda)} \rho dV. \quad 5.$$

In addition to being bound by  $\lambda$  iso-surfaces ( $\partial\Omega_\lambda$ ), the water mass can be bounded by the sea surface and defined for a specific ocean basin or another geographical delineation, such as being above the winter mixed layer. That is, the water mass can have an outcrop area ( $\partial\Omega_{\text{out}}$ , the region where  $\Omega$  meets the sea surface), and it can have an interior boundary surface area ( $\partial\Omega_{\text{int}}$ , where  $\Omega$  meets the interior boundary), both bounded between  $\lambda - \Delta\lambda/2$  and  $\lambda + \Delta\lambda/2$  contours (see **Figure 3**). We write the union of these boundaries as

$$\partial\Omega = \partial\Omega_{\text{out}} + \partial\Omega_{\text{int}} + \partial\Omega_{\lambda+\Delta\lambda/2} + \partial\Omega_{\lambda-\Delta\lambda/2}. \quad 6.$$

The mass transport across the interior boundary,  $\partial\Omega_{\text{int}}(\lambda)$ , is written

$$\Delta\Psi = \iint_{\partial\Omega_{\text{int}}(\lambda)} \rho(\mathbf{u} - \mathbf{u}_b) \cdot \hat{\mathbf{n}}_b dA, \quad 7.$$

where  $dA$  is the area element on the boundary,  $\hat{\mathbf{n}}_b$  is the unit normal oriented outward from the water mass across the interior boundary (e.g., across a transcontinental section or the base of the mixed layer), and  $\mathbf{u}_b$  is the velocity of a point on the boundary. We choose signs so that  $\Delta\Psi(\lambda) > 0$  indicates that water leaves the domain. For a global mass budget,  $\partial\Omega_{\text{int}}$  disappears, and  $\Delta\Psi = 0$ . For models with parameterized eddy-induced mass transport, it is important that  $\mathbf{u}$  represent the residual mean velocity since that is the velocity advecting seawater mass and tracers (Gent et al. 1995, McDougall & McIntosh 2001).

We provide an analogous treatment in cases where the water mass outcrops at the ocean surface. Here, there are generally air-sea and ice-sea mass fluxes across the outcrop interface  $\partial\Omega_{\text{out}}$ , with the integrated flux (i.e., the boundary mass transport) given by

$$\Delta W(\lambda) = \iint_{\partial\Omega_{\text{out}}(\lambda)} (P - E + R + I + Ae) dA, \quad 8.$$

where evaporation ( $E$ , positive out of the ocean), precipitation ( $P$ , positive into the ocean), river runoff ( $R$ , positive into the ocean), ice melt ( $I$ , positive into the ocean), and aeolian deposition of salt ( $Ae$ ) are provided as mass fluxes (mass per unit time per unit area) crossing the ocean surface ( $E$ ,  $P$ , and  $Ae$ ), entering the ocean laterally ( $R$ ), or both ( $I$ ). We choose a sign convention following **Figure 3**, so that  $\Delta W(\lambda) > 0$  means that mass is added to the budget domain.

The above definitions lead to the mass budget for the volume  $\Delta V$ :

$$\Delta F \equiv \underbrace{\frac{\partial(\Delta M)}{\partial t}}_{\text{trend plus outflow}} + \Delta\Psi = \underbrace{G(\lambda - \Delta\lambda/2) - G(\lambda + \Delta\lambda/2)}_{\text{water mass formation into } (\lambda - \Delta\lambda/2, \lambda + \Delta\lambda/2)} + \Delta W. \quad 9.$$



Here,  $\Delta F$  is defined as the layer WMF (Nurser et al. 1999). It measures the mass of seawater produced as a result of mass fluxes ( $\Delta W$ ) and the convergence of WMT ( $G$ ).  $\Delta F$  also equals the temporal change in layer mass ( $\partial \Delta M / \partial t$ ) plus the outflow of mass crossing the interior domain boundary via ocean circulation ( $\Delta \Psi$ ).

Taking the limit as the layer thickness becomes infinitesimal,  $\Delta \lambda \rightarrow 0$ , leads to the continuum WMF equation

$$\frac{\partial}{\partial \lambda} \left( \frac{\partial M}{\partial t} + \Psi \right) = \frac{\partial}{\partial \lambda} \left( -G + W \right) \implies \Psi = -G + W - \frac{\partial M}{\partial t}, \quad 10.$$

where we have made use of relations derived in Appendix 1 (Section 7) for taking the limit. The right-hand equality results from integrating from a reference value  $\lambda_0$  to an arbitrary layer  $\lambda$ , meaning  $M$ ,  $W$ ,  $G$ , and  $\Psi$  are integrated over all volume below  $\lambda$ .

## 2.4. Application of Water Mass Formation to Obtain a Circulation

Equation 10 expresses the total along-surface mass transport  $\Psi(\lambda)$  below the  $\lambda$  surface in terms of sources of  $\lambda$  (through  $G$ ), a surface mass flux ( $W$ ), and a trend ( $\partial M / \partial t$ ). In the special case of a steady-state layer ( $\partial M / \partial t = 0$ ) and a zero surface mass flux ( $W = 0$ ), the along-surface mass transport is determined only by WMT:  $\Psi(\lambda) = -G(\lambda)$ .

If the interior boundary,  $\partial \Omega_{\text{int}}$  (Equation 7), is the base of the mixed layer, then  $\Psi$  measures the mass of water subducting into the interior from the mixed layer (see Section 4.6). If  $\partial \Omega_{\text{int}}$  is a meridional section, then  $\Psi$  is the accumulated transport of mass across that section (Ferrari & Ferreira 2011). When we apply this approach to a meridional section and buoyancy (recall the pancake analogy in Section 1.3), this formulation allows for a quantification of the meridional-buoyancy overturning circulation from buoyancy fluxes alone (see Section 3.4). As ocean circulation is difficult to directly measure on large scales, box-inverse methods (Wunsch 1978, Ganachaud & Wunsch 2000) have been used to obtain estimates of circulation from hydrography measurements. The WMT framework provides a complementary method to estimate circulation based on layer budgets.

## 3. THE BUOYANCY-BASED WATER MASS TRANSFORMATION FRAMEWORK

We now specialize the previous general discussion to buoyancy,  $\lambda = \gamma$ , where  $\gamma$  defines neutral surfaces. The buoyancy-based WMT analysis provides a framework to directly quantify the ocean's dianeutral transport and relate it to its epineutral transport ( $\Psi$ ; see Section 2.4), thus directly linking to circulation and related property transport (recall the pancake analogy from Section 1.3).

### 3.1. Defining Buoyancy Surfaces

We use neutral surfaces to partition the ocean fluid. The dianeutral unit vector is defined according to the gradient of locally referenced potential density  $\rho_l$  (McDougall et al. 2014):<sup>2</sup>

$$\hat{n}_\rho = \frac{\nabla \rho_l}{|\nabla \rho_l|}, \quad \text{where} \quad \nabla \rho_l = \rho(-\alpha \nabla \Theta + \beta \nabla S). \quad 11.$$

<sup>2</sup>McDougall et al. (2014) define  $\hat{n}_\rho$  with a minus sign relative to Equation 11. However, Equation 11 accords with conventions in the WMT literature, with  $\hat{n}_\rho$  pointing toward increasing density (see Section 2.1).

Here,  $\rho_l$  is the in situ density  $\rho$ , referenced to the  $S$ ,  $\Theta$ , and pressure ( $P$ ) of the location where the dianeutral vector is defined, and  $\alpha = \alpha(S_\Lambda, \Theta, P)$  and  $\beta = \beta(S_\Lambda, \Theta, P)$  are the thermal and haline expansion coefficients, respectively (units of  $K^{-1}$  and  $S^{-1}$ ).

Due to a nonzero neutral helicity, which is an effect of the nonlinear dependence of  $\rho$  on  $S$ ,  $\Theta$ , and  $P$ , the differential increment tracking neutral directions is path dependent for a line integration following neutral directions (McDougall & Jackett 1988). Path dependence in turn means that there is no globally defined surface whose tangent at each point is parallel to neutral directions. Therefore, we have access only to a local definition of a neutral surface, i.e., the neutral tangent plane (McDougall 1987a). From the accumulation of neutral tangent planes, an approximate continuous neutral surface  $\gamma$  can be constructed for purposes of WMT analysis. The material evolution of  $\gamma$  is written (McDougall & Jackett 2005, Iudicone et al. 2008b)

$$\dot{\gamma} = (b\gamma/\rho) \dot{\rho}_l = b\gamma (-\alpha \dot{\Theta} + \beta \dot{S}) = \text{boundary-layer fluxes} + \text{irreversible mixing}, \quad 12.$$

which results from changes in  $S$  and  $\Theta$  arising from interior mixing processes and boundary fluxes [Appendix 2 (Section 8)]. This expression uses  $\rho_l$  to define  $\dot{\gamma}$  and will be inserted into Equation 4 to obtain the dianeutral WMT. The dimensionless ratio  $b = |\nabla\gamma|/|\nabla\rho_l|$  is required to construct an approximate global neutral surface from surfaces that are only locally defined. The error made by this approximation to the neutral direction is small (McDougall & Jackett 1988) except in the Southern Ocean (Klocker & McDougall 2010a,b). Practical examples of  $\gamma$  are the  $\omega$  surfaces of Klocker et al. (2009) and neutral density surfaces  $\gamma^n$  of Jackett & McDougall (1997). We make use of a generic symbol  $\gamma$ , anticipating improved neutral variables in the future.<sup>3</sup>

To avoid complexities related to the construction of  $\gamma$  surfaces, potential density  $\rho_\Theta = \rho(S, \Theta, P = P_r)$  is commonly used as an alternative to approximate neutral directions for WMT-related studies (Speer & Tziperman 1992, Marshall et al. 1999, Marsh et al. 2000). At the fixed reference pressure  $P_r$ , the potential density  $\rho_\Theta$  is exactly aligned with the neutral tangent plane. However, the further away the potential density surface is removed from its reference pressure, the less accurately it will represent the neutral direction at that location. Furthermore, using a constant reference pressure removes density changes related to thermobaric processes (detailed in Section 3.3).

As a rule of thumb, potential density reasonably approximates a neutral surface within a vertical extent of approximately 250–500 m from its reference pressure. There is no suitable potential density field for studying WMT over all depths, so a more accurate  $\gamma$ -like approximation is favored (Iudicone et al. 2008b, Groeskamp et al. 2016a).

### 3.2. Boundary Fluxes of Salt and Heat

At the ocean boundary layers (air-sea, ice-sea, and earth-sea), there are several sources that can alter the ocean's salt and heat content, which in turn leads to material time changes in  $\gamma$  and a corresponding WMT. Here, we present the boundary-layer sources, with further details provided in Appendix 2 (Section 8, particularly Equations 50 and 51 for salinity and temperature, respectively).

**3.2.1. Salt and heat fluxes due to a mass influx.** At the ocean boundaries, there can be a mass influx ( $kg\ m^{-2}\ s^{-1}$ ) given by  $Q_m = E - P + R + I + Ae$  (Equation 8, **Figures 2** and **3**). Each

<sup>3</sup>The  $\omega$  surfaces are the most accurate approximation of  $\gamma$ , but they are computationally expensive and not uniquely defined;  $\gamma^n$  is regularly used in practice but is not defined poleward of 64°N or for some inland seas.



component of the mass flux has a salinity and temperature that generally differ from those of the ocean  $S$  and  $\Theta$  where it enters, thereby changing the ocean density. We write  $S_m$  and  $\Theta_m$  as the mass-flux-weighted average of the salinity and temperature of the various components, leaving

$$F_{\text{mass}}^{\rho} = \underbrace{-\alpha Q_m (\Theta_m - \Theta) \delta(z - \eta)}_{\text{from heat carried by mass}} + \underbrace{\beta Q_m (S_m - S) \delta(z - \eta)}_{\text{from salt carried by mass}}. \quad 13.$$

The density source  $F_{\text{mass}}^{\rho}$  ( $\text{kg m}^{-3} \text{ s}^{-1}$ ) contains a Dirac delta function,  $\delta(z - \eta)$ , with units of inverse length and with  $z = \eta(x, y, t)$  the ocean free surface height. The delta function is a shorthand for the vertical convergence of the boundary flux at the ocean surface [Appendix 2 (Section 8)]. Often, the temperature of the mass flux equals the ocean temperature ( $\Theta = \Theta_m$ ), making the related heat flux term absent in Equation 13. That is, ocean temperature is unaffected by the boundary-layer mass flux if  $\Theta = \Theta_m$ , although ocean heat content changes. By contrast, the air-sea mass flux generally has a vanishing salinity,  $S_m = 0$ , making  $F_{\text{mass}}^{\rho} = -Q_m \beta S \delta(z - \eta)$  an important term in the density budget.

**3.2.2. Direct salinity and heat fluxes at the ocean boundaries.** There are generally direct sources of salinity and heat at the ocean boundary that are unrelated to the boundary mass flux. Heat fluxes at the ocean surface,  $F_Q$  (positive into the ocean,  $\text{W m}^{-2}$ ), include the net heat flux due to longwave radiation as well as turbulent fluxes associated with latent and sensible heat. There can be salinity fluxes,  $F_S$  ( $\text{g m}^{-2} \text{ s}^{-1}$ ), associated with sea ice as well as salinity relaxation commonly used in ocean/sea-ice models. We are left with the surface boundary-layer flux of density

$$F_{\text{surface}}^{\rho} = \left( -\frac{\alpha}{C_p} F_Q + \beta F_S \right) \delta(z - \eta). \quad 14.$$

Shortwave radiation is separated from the term  $F_{\text{surface}}^{\rho}$  since shortwave radiation penetrates into the upper-ocean layer as a function of the optical color (determined largely by biology) (Lewis et al. 1983, 1990). It is thus common to apply an exponential decay to penetrative shortwave radiation depending on the chlorophyll  $a$  distribution (Morel & Antoine 1994). The penetration of shortwave radiation changes the depth and density of transformed water, thus affecting ocean circulation (Sweeney et al. 2005, Iudicone et al. 2008b) and climate (Gnanadesikan & Anderson 2009). The change in  $\rho$  due to penetrative shortwave radiation is written

$$F_{\text{swr}}^{\rho} = \frac{\alpha}{C_p} \nabla \cdot \mathbf{J}_Q^{\text{swr}}, \quad 15.$$

where  $\mathbf{J}_Q^{\text{swr}}$  is the vertically redistributed shortwave radiative heat flux ( $\text{W m}^{-2}$ ).

Finally, geothermal heat fluxes  $F_{\text{geo}} \geq 0$  ( $\text{W m}^{-2}$ ) provide a direct subsurface input of heat at the ocean bottom [ $z = -H(x, y)$ ]:

$$F_{\text{geo}}^{\rho} = -\frac{\alpha}{C_p} F_{\text{geo}} \delta(z + H). \quad 16.$$

De Lavergne et al. (2015) pointed to the importance of geothermal heating for transformation of Antarctic Bottom Water into lighter waters.

**3.2.3. Buoyancy water mass transformation induced by boundary salt and heat fluxes.** The combined effect of all boundary fluxes ( $F_{\text{bdy}}^{\rho}$ ) is then given by

$$F_{\text{bdy}}^{\rho} = F_{\text{mass}}^{\rho} + F_{\text{surface}}^{\rho} + F_{\text{swr}}^{\rho} + F_{\text{geo}}^{\rho}. \quad 17.$$

Our convention is chosen so that  $F_{\text{bdy}}^{\rho} > 0$  leads to an increase in ocean density, which in turn decreases buoyancy. Buoyancy increases where relatively warm ( $\Theta_m > \Theta$ ) and fresh ( $S_m < S$ ) water

enters through a positive mass flux ( $Q_m > 0$ ). Buoyancy also increases where the net turbulent and radiative surface heat fluxes are positive ( $F_Q > 0$ ), and it increases where penetrative shortwave radiation converges ( $-\nabla \cdot \mathbf{J}_Q^{\text{short}} > 0$ ). Geothermal heating is always a source of bottom buoyancy since  $F_{\text{geo}} \geq 0$ . Finally, buoyancy increases where the salinity flux is negative ( $F_S < 0$ ). The net WMT derived from the boundary flux sources of Equation 17 is given by

$$G_{\text{bdy}}(\gamma) = \frac{\partial}{\partial \gamma} \iiint_{\gamma' \leq \gamma} \gamma' b F_{\text{bdy}}^\rho dV. \quad 18.$$

By construction (see Equation 2), positive values of  $G_{\text{bdy}}(\gamma)$  mean that the water becomes more dense, and negative values mean that it becomes less dense. Note that the prime symbol on  $\gamma'$  merely indicates the variable over which it is integrated (see Equations 4 and 44).

### 3.3. Diffusive Fluxes of Salt and Heat

Irreversible mixing in the ocean takes place at the millimeter scale, acting to dissipate property gradients. This mixing is generally represented by downgradient molecular diffusion, i.e., diffusion induced by Brownian motion (Einstein 1905). The molecular diffusivity of matter (e.g., salt) in seawater is roughly  $10^{-9} \text{ m}^2 \text{ s}^{-1}$ , whereas the molecular thermal diffusivity is roughly 100 times greater (it is easier to diffuse heat than matter) (Gill 1982). Reversible stirring by turbulent eddies greatly increases the magnitude of property gradients upon which molecular diffusion acts (Eckart 1948, Garrett 2001, Nakamura 2001), thereby increasing the total amount of irreversible mixing in the ocean. Turbulent stirring by eddies commonly occurs at spatial scales too small to resolve in circulation models. Consequently, the mixing induced by eddy stirring must be parameterized. Motivated by molecular diffusion, and following the pioneering work of Taylor (1921), a common parameterization makes use of a diffusive closure with an eddy diffusivity that is far larger than molecular values.

Mixing induced by small-scale eddies,  $\mathcal{O}(\text{centimeters} - \text{meters})$ , is associated with, among other processes, gravitation instability, shear instability, and breaking internal gravity waves (MacKinnon et al. 2013), as well as a suite of boundary-layer processes (Large et al. 1994). This enhanced mixing is commonly parameterized by isotropic turbulent diffusion with diffusivity  $D$  and corresponding downgradient tracer flux  $-DV\lambda$ . Notably, the vertical component dominates this diffusive flux in most oceanographic applications in the presence of vertical stratification. The magnitude of the eddy diffusivity is typically  $\mathcal{O}(10^{-3}-10^{-2} \text{ m}^2 \text{ s}^{-1})$  in boundary layers and  $\mathcal{O}(10^{-5} \text{ m}^2 \text{ s}^{-1})$  in the quiescent ocean interior (Polzin et al. 1997, Whalen et al. 2012, Waterhouse et al. 2014).

Mesoscale eddies, with size  $\mathcal{O}(20-200 \text{ km})$ , preferentially stir tracers along neutral directions. The resulting mixing is commonly parameterized by downgradient diffusion along neutral directions using a mesoscale eddy diffusivity  $K_N$ . The associated downgradient neutral diffusive tracer flux is written  $-K_N \nabla_N \lambda$ , where  $\nabla_N$  is the gradient along a neutral direction [see Appendix 2 (Section 8.3), Redi 1982, Griffies et al. 1998, and McDougall et al. 2014]. When feeling the geometric constraints of the surface boundary, mesoscale stirring leads to horizontally oriented mixing across outcropped density surfaces (Tandon & Garrett 1997, Treguier et al. 1997, Ferrari et al. 2008). This mixing is parameterized by downgradient horizontal diffusion with an eddy diffusivity  $K_H$ . The horizontal downgradient diffusive flux is given by  $-K_H \nabla_H \lambda$ , where  $\nabla_H$  is the horizontal gradient. The magnitude for  $K_N$  and  $K_H$  is typically  $\mathcal{O}(10^2-10^3 \text{ m}^2 \text{ s}^{-1})$  in the ocean interior and can rise to  $\mathcal{O}(10^4 \text{ m}^2 \text{ s}^{-1})$  in the ocean surface layer (Abernathy & Marshall 2013, Klocker & Abernathy 2013, Cole et al. 2015). Although the small-scale isotropic diffusivity  $D$  is much smaller than  $K_N$  and  $K_H$ , the diffusivity  $D$  multiplies the generally larger vertical gradients crossing density layers and thus supports WMT and the induced ocean circulation (Munk 1966, Munk & Wunsch 1998).



As detailed in Appendix 2 (Section 8.3), the material time evolution of locally referenced potential density arising from salt and heat diffusion can be decomposed as

$$(\dot{\rho}_l)_{\text{mix}} = (\dot{\rho}_l)_{\text{hor}} + (\dot{\rho}_l)_{\text{iso}} + \text{Cab} + \text{Thb}. \quad 19.$$

Here,  $(\dot{\rho}_l)_{\text{hor}}$  and  $(\dot{\rho}_l)_{\text{iso}}$  are changes due to horizontal and isotropic diffusion, respectively ( $\text{kg m}^{-3} \text{s}^{-1}$ ). The effect on  $\rho_l$  from neutral diffusion is given by cabbeling (Cab) and thermobaricity (Thb), which arise from nonlinearities in the equation of state (Witte 1902; Foster 1972; McDougall 1984, 1987b). Both processes have a significant effect on WMT (Marsh 2000, Talley & Yun 2001, Iudicone et al. 2008b, Urakawa & Hasumi 2012, Groeskamp et al. 2016a) and the resulting dianeutral transports. In contrast to using  $\gamma$ , when one uses  $\rho_\Theta$ , there is no contribution from thermobaricity (IOC et al. 2010). Inserting the mixing processes into the WMT equation gives

$$G_{\text{mix}}(\gamma) = \frac{\partial}{\partial \gamma} \iiint_{\gamma' \leq \gamma} \gamma' b (\dot{\rho}_l)_{\text{mix}} \, dV. \quad 20.$$

### 3.4. Total Dianeutral Transport Quantified in Terms of Water Mass Transformation

The sum of Equations 17 and 19 provides the material derivative of  $\rho_l$ ,

$$\dot{\rho}_l = \underbrace{F_{\text{mass}}^\rho + F_{\text{surface}}^\rho + F_{\text{swr}}^\rho + F_{\text{geo}}^\rho}_{\text{boundary fluxes}} + \underbrace{(\dot{\rho}_l)_{\text{hor}} + (\dot{\rho}_l)_{\text{iso}} + \text{Cab} + \text{Thb}}_{\text{diffusive fluxes}}, \quad 21.$$

from which the total dianeutral transport (quantified by WMT) is the sum of Equations 18 and 20:<sup>4</sup>

$$G(\gamma) = \frac{\partial}{\partial \gamma} \iiint_{\gamma' \leq \gamma} \gamma' b \dot{\rho}_l \, dV \quad 22a.$$

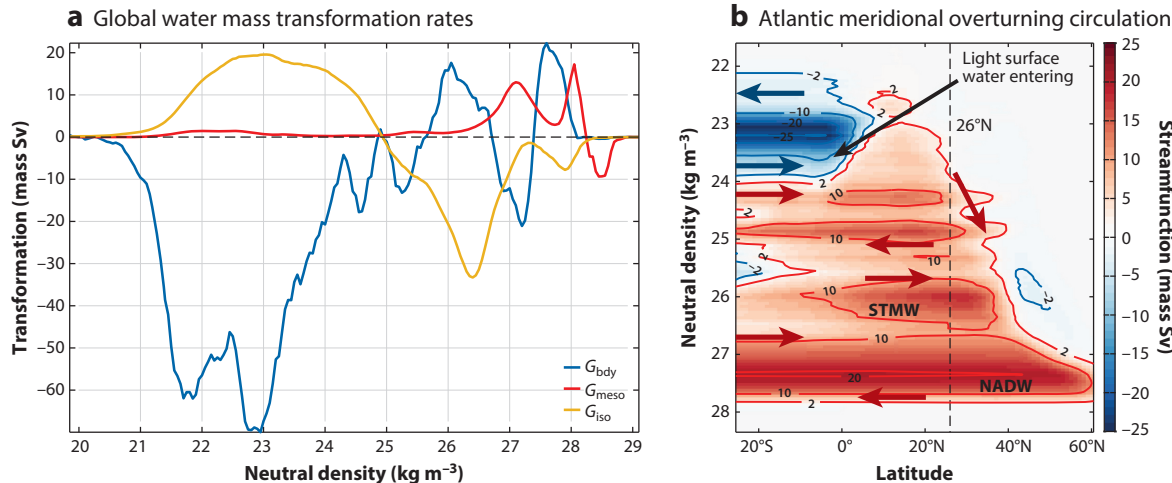
$$= \underbrace{G_{\text{mass}} + G_{\text{surface}} + G_{\text{swr}} + G_{\text{geo}}}_{\text{boundary fluxes } G_{\text{bdy}}} + \underbrace{G_{\text{hor}} + G_{\text{iso}} + G_{\text{cab}} + G_{\text{thb}}}_{\text{diffusive fluxes } G_{\text{mix}}}. \quad 22b.$$

$G$  is represented as a sum of physical process influencing the material derivative of density (Equation 21). For example,  $G_{\text{mass}}$  is the contribution of the surface mass flux and can be calculated by replacing  $\dot{\rho}_l$  with  $F_{\text{mass}}^\rho$  in Equation 22a.

**Figure 4a** compares global WMT rates due to air-sea fluxes ( $G_{\text{bdy}}$ ) and mixing ( $G_{\text{mix}}$ ) in neutral density ( $\gamma^n$ ) phase space. The mixing is split up into mesoscale mixing ( $G_{\text{hor}} + G_{\text{cab}} + G_{\text{thb}}$ ) and small-scale mixing ( $G_{\text{iso}}$ ). Air-sea fluxes generally add buoyancy to light water and remove buoyancy from dense water, thus producing the extremes in the globally observed water mass distribution (Large & Nurser 2001). Mixing acts to reduce extremes, therefore generally showing an opposite structure.

**Figure 4b** shows the corresponding Atlantic meridional overturning circulation (AMOC). The AMOC is calculated by applying Equation 10 from 60°N to 30°S in the Atlantic and partitioned by latitude. The AMOC shows both a shallow and deep overturning, with light water entering the domain and transforming into Subtropical Mode Water and North Atlantic Deep Water (red cell in **Figure 4b**). Additionally, equatorial upwelling of 23 mass sverdrups (Sv) is transformed into

<sup>4</sup>McDougall (1984) and section A.23 of IOC et al. (2010) define the WMT equation to determine the change in  $\Theta$  (or any tracer) of a fluid element as it changes when measured along a neutral surface. This definition is distinct from our usage, which is based on Walin (1982) and is applied to neutral density in Equation 22a.

**Figure 4**

(a) Global annual mean  $\gamma^n$ -based water mass transformation for air-sea fluxes ( $G_{\text{bdy}}$ , blue line), mesoscale mixing ( $G_{\text{meso}}$ , red line), and isotropic small-scale mixing ( $G_{\text{iso}}$ , yellow line). Here, 1 mass sverdrup (Sv) =  $1 \times 10^9 \text{ kg s}^{-1}$ . (b) The Atlantic meridional overturning circulation as calculated per Equation 10. For the calculations, we used data from *World Ocean Database 2013* (Boyer et al. 2013) combined with Gibbs Seawater software (McDougall & Barker 2011). For air-sea fluxes, we used the Coordinated Ocean Research Experiments (CORE) data set (Large & Yeager 2009) and applied a shortwave radiation redistribution according to Ohlmann (2003). For simplicity, we used constant diffusivities of  $K_H = K_N = 500 \text{ m}^2 \text{ s}^{-1}$  and  $D = 1 \times 10^{-5} \text{ m}^2 \text{ s}^{-1}$ . Abbreviations: NADW, North Atlantic Deep Water; STMW, Subtropical Mode Water.

lighter water ( $\gamma^n = 23\text{--}24 \rightarrow 22\text{--}23 \text{ kg m}^{-3}$ ; blue cell in **Figure 4b**). Insights gained by analyzing the overturning streamfunction in latitude-density space were emphasized by Döös & Webb (1994) and Hirst et al. (1996), and this analysis now represents a standard model diagnostic (e.g., Danabasoglu et al. 2014, Farneti et al. 2015). The peak North Atlantic Deep Water transport is located at approximately 50°N, with a magnitude of approximately 20 mass Sv, closely resembling the AMOC obtained in these ocean modeling studies.

In **Figure 4a**, constant diffusivities are applied, serving to illustrate the expected circulation structures and magnitude of WMT rates. With improved mixing estimates obtained from other WMT studies (Lumpkin & Speer 2007, Zika et al. 2010, Groeskamp et al. 2017), future work will provide more accurate WMT budgets. Related observation-based estimates of the AMOC can then offer a critical reference for ocean model evaluation.

#### 4. GENERALIZING THE WATER MASS TRANSFORMATION FRAMEWORK TO INCLUDE TRACERS

Let  $c$  be the concentration of a dissolved trace constituent (e.g., nitrate, carbon, or salt), given by the ratio of the tracer mass to seawater mass (e.g., gram of tracer per kilogram of seawater). Also allow for  $c$  to have a particulate component, such as for certain biogeochemical tracers. The ocean circulation moves the tracer around through advection, while the dissolved tracer may experience material changes ( $\dot{c}$ , g kg<sup>-1</sup> s<sup>-1</sup>) due to turbulent mixing processes with its surroundings ( $d_c$ ), as well as tracer boundary fluxes ( $f_c$ ), biogeochemical processes ( $b_c$ ), and the movement of tracer relative to the fluid velocity, such as a sinking velocity for particulate matter ( $z_c$ ), such that

$$\rho \dot{c} \equiv f_c + d_c + b_c + z_c. \quad 23.$$



**Particulate velocity:**  
the velocity of the  
particulate  
components of a  
tracer  $c$

We can include the material tracer changes,  $\rho \dot{c}$ , in the neutral density-based WMT framework of Section 3. As such,  $\gamma$  partitions the ocean into layers within which we examine tracer budgets. This approach unlocks a generalized framework to separately quantify the effect of circulation through the material changes of  $\gamma$  (from boundary buoyancy fluxes and mixing) and to quantify the effects of material tracer changes on the ocean's tracer distribution. This section builds on the theoretical developments described by Iudicone et al. (2008c, 2011), here also including the air-sea mass fluxes and particulate velocity (through  $z_c$ ).

#### 4.1. Ocean Tracer Circulation

As detailed in Appendix 3 (Section 9, Equation 61), there are two ways in which the mass of tracer,  $\Delta C$ , within a domain  $\Omega$  can change: (a) material tracer changes (the first term in Equation 24) and (b) water entering the layer with a nonzero tracer concentration  $c$  (second term), thus rendering (mass per unit time)

$$\frac{d(\Delta C)}{dt} = \underbrace{\iiint_{\Omega} \rho \dot{c} dV}_{\text{tracer sources}} - \underbrace{\iint_{\partial\Omega} \rho c (\mathbf{u} - \mathbf{u}_b) \cdot \hat{\mathbf{n}}_b dA}_{\text{dia-boundary transport}}. \quad 24.$$

Here,  $\dot{c}$  is the material time change of the tracer concentration (Equation 23),  $\mathbf{u}_b$  is the velocity of the boundary  $\partial\Omega$  (Equation 6), and  $\hat{\mathbf{n}}_b$  is a unit normal that orients the boundary. Treatment of the dia-boundary integral is kinematic, with the transport of seawater mass across a boundary generally bringing with it a nonzero tracer content. Additional cross-boundary transport occurs through nonadvection processes (such as diffusion) and biogeochemical sources.

#### 4.2. Tracer Changes by Mass Fluxes Through Bounding Surfaces

In this section, we detail how a tracer can change within a layer due to mass transport across the layer boundaries (the second term on the right-hand side of Equation 24).

**4.2.1. Dianeutral tracer transport by water mass transformation (through  $\partial\Omega_\gamma$ ).** The total transport of material across a neutral surface depends on the concentration of material within the water when it changes density by WMT. The dianeutral tracer transport through a surface of constant  $\gamma$  is thus given by (using Equation 22a)

$$E_C(\gamma) = \iint_{\partial\Omega_\gamma} \rho c u_\gamma^{\text{dia}} dA = \frac{\partial}{\partial \gamma} \iiint_{\gamma' \leq \gamma} b c \gamma' \dot{\rho}_l dV \quad 25a.$$

$$= \underbrace{E_C^{\text{mass}} + E_C^{\text{surf}} + E_C^{\text{swr}} + E_C^{\text{geo}}}_{\text{input from boundary fluxes } E_C^{\text{bdy}}} + \underbrace{E_C^{\text{hor}} + E_C^{\text{iso}} + E_C^{\text{cab}} + E_C^{\text{thb}}}_{\text{input from diffusive fluxes } E_C^{\text{mix}}}. \quad 25b.$$

As with the transformation rate  $G$ , the dianeutral tracer transport  $E_C$  in Equation 25b is a linear sum of contributions from physical processes influencing the material derivative of density (Equation 21). These processes are calculated using Equation 22a by replacing  $\dot{\rho}_l$  with the appropriate term from Equation 25a. Notably, if  $c$  is a constant along a neutral surface, then  $E_C(\gamma) = cG(\gamma, t)$ . [For practical implementation details as related to  $G(\gamma)$ , see Equation 48.]

**4.2.2. Tracer mass flux through the outcrop (through  $\partial\Omega_{\text{out}}$ ).** In analogy with heat and salt fluxes (Equation 13), the outcrop area exposes the domain to mass fluxes that may have a tracer

concentration  $c_m$  that differs from the concentration where it enters the ocean:

$$\Delta F_C^{\text{mass}} = \iint_{\partial\Omega_{\text{out}}} Q_m (c_m - c) dA. \quad 26.$$

**4.2.3. Tracer advection through the interior boundary (through  $\partial\Omega_{\text{int}}$ ).** If there is an open boundary between the neutral surfaces, then tracer may be advected out of the domain:

$$\Delta\Psi_C = \iint_{\partial\Omega_{\text{int}}} \rho c (\mathbf{u} - \mathbf{u}_b) \cdot \hat{\mathbf{n}}_b dA. \quad 27.$$

Note that if  $c$  is constant within the layer, then  $\Delta\Psi_C = c \Delta\Psi$ . We further detail this term in Section 4.6 for the special case of subduction and ventilation from the mixed layer.

### 4.3. Material Tracer Changes

In this section, we detail how a tracer changes within a layer due to material time changes within the layer (the first term on the right-hand side of Equation 24).

**4.3.1. Diffusive tracer fluxes (through  $\partial\Omega_{\text{int}}$  and  $\partial\Omega_y$ ).** Tracers may diffuse just like heat and salt [Section 3.3 and Appendix 2 (Section 8.3)], so that we can define  $\mathbf{J}_c = -\rho \mathbf{K} \nabla c$ . The diffusivity tensor  $\mathbf{K}$  can be split into different mixing processes. Integrating this over the entire volume  $\Omega$  leaves a net transport through the bounding surfaces:

$$\Delta M_C(\gamma) = - \underbrace{\iint_{\partial\Omega_{y-\Delta\gamma/2}} \mathbf{J}_c \cdot \mathbf{n}_{y-\Delta\gamma/2} dA}_{M_C^{\text{dia}}(y-\Delta\gamma/2)} + \underbrace{\iint_{\partial\Omega_{y+\Delta\gamma/2}} \mathbf{J}_c \cdot \mathbf{n}_{y+\Delta\gamma/2} dA}_{-M_C^{\text{dia}}(y+\Delta\gamma/2)} - \underbrace{\iint_{\partial\Omega_{\text{int}}} \mathbf{J}_c \cdot \hat{\mathbf{n}}_b dA}_{\Delta M_C^{\text{int}}}. \quad 28.$$

Here,  $M_C^{\text{dia}}$  is the contribution from the dianeutral diffusive tracer flux. Note that there is no tracer diffusion through the ocean surface  $\partial\Omega_{\text{out}}$ , and the neutral tracer diffusive flux is along the neutral direction, so it does not have a component in the dianeutral direction.  $\Delta M_C^{\text{int}}$  is the tracer diffusion across the interior boundary. It is determined by neutral diffusion in cases where the outward normal to the outflow boundary is parallel to the neutral direction.

**4.3.2. Boundary-layer tracer fluxes.** The boundary-layer tracer flux provides a direct input of tracer into the domain through boundary-layer processes:

$$\Delta F_C^{\text{tracer}} = \iiint_{\Omega} f_c dV. \quad 29.$$

For most types of tracer, Equation 29 reduces to an integral of air-sea tracer fluxes along the outcrop area ( $\partial\Omega_{\text{out}}$ ). However, certain tracers may have large interior sources as well (e.g.,  ${}^3\text{He}$  sources at ocean ridges) (Lupton & Craig 1981, Jamous et al. 1992).

**4.3.3. Biogeochemical processes.** If  $c$  is a reactive tracer, then we define  $b_c$  as all the biological and chemical processes that lead to a change in the tracer concentration  $C$  throughout the whole domain:

$$\Delta B_C = \iiint_{\Omega} b_c dV. \quad 30.$$

**4.3.4. Particulate transport (through  $\partial\Omega_{\text{int}}$  and  $\partial\Omega_y$ ).** Consider a tracer  $c$  that consists of particulate matter that is diluted enough that it does not significantly affect the seawater density



and abundant enough that it can be treated as a continuum. Examples are living and dead organisms, fecal pellets, microplastics, aggregates, and the particulate matter that comprises the biological carbon pump. Such particulate tracers can have a particulate velocity  $\mathbf{u}_c$ , which in turn adds the convergence of a particulate matter flux  $z_c = -\nabla \cdot (c \rho \mathbf{u}_c)$  to the material evolution equation (Equation 23). Note that an initially uniform tracer concentration is modified where  $\nabla \cdot (\rho \mathbf{u}_c) \neq 0$  (e.g., regions where particulates accumulate). A common example is a vertical sinking velocity,  $\mathbf{u}_c = \hat{\mathbf{z}} w_{\text{sink}}$ , causing  $c$  particles to vertically settle through the water column (e.g., Aumont et al. 2015). We calculate the convergence of particulate transport within  $\Omega$  using  $z_c = -\nabla \cdot (c \rho \mathbf{u}_c)$ , which yields (following Equation 28)

$$\Delta Z_C(\gamma) = - \underbrace{\iint_{\partial\Omega_{\gamma-\Delta\gamma/2}} \rho c \mathbf{u}_c \cdot \mathbf{n}_{\gamma-\Delta\gamma/2} dA}_{Z_C^{\text{dia}}(\gamma-\Delta\gamma/2)} + \underbrace{\iint_{\partial\Omega_{\gamma+\Delta\gamma/2}} \rho c \mathbf{u}_c \cdot \mathbf{n}_{\gamma+\Delta\gamma/2} dA}_{-Z_C^{\text{dia}}(\gamma+\Delta\gamma/2)} - \underbrace{\iint_{\partial\Omega_{\text{int}}} \rho c \mathbf{u}_c \cdot \hat{\mathbf{n}}_b dA}_{\Delta Z_C^{\text{int}}}. \quad 31.$$

The first and second terms arise from transport through the bounding neutral surfaces, and the third term is due to transport through the interior boundary.

#### 4.4. Total Tracer Budget

Combining all terms renders

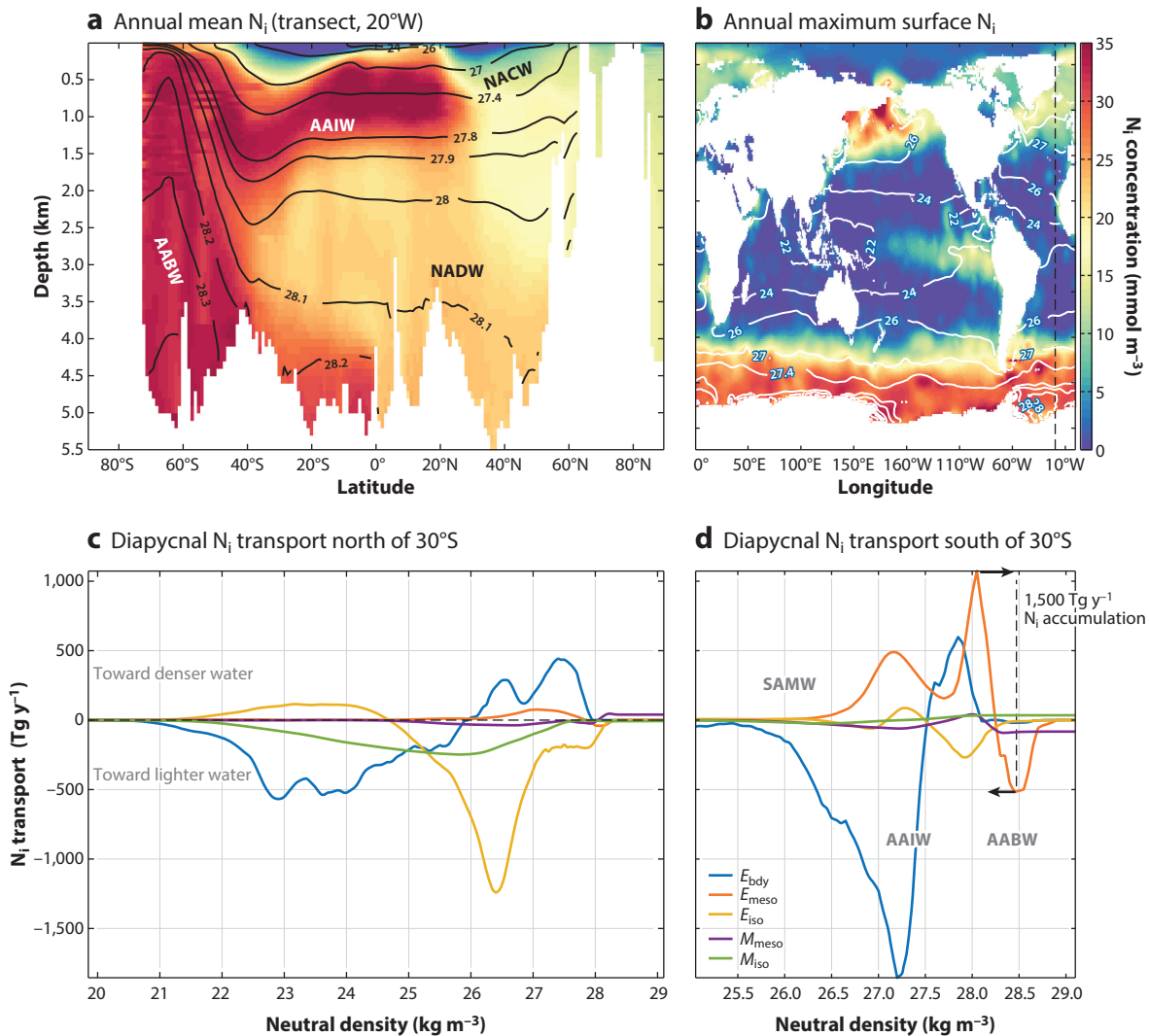
$$\begin{aligned} \frac{d(\Delta C)}{dt} &= \underbrace{E_C(\gamma - \Delta\gamma/2) - E_C(\gamma + \Delta\gamma/2) + \Delta F_C^{\text{mass}} + \Delta\Psi_C}_{\text{dia-boundary transport}} \\ &+ \underbrace{M_C^{\text{dia}}(\gamma - \Delta\gamma/2) - M_C^{\text{dia}}(\gamma + \Delta\gamma/2) + \Delta M_C^{\text{int}} + \Delta F_C^{\text{tracer}} + \Delta B_C}_{\text{material tracer changes}} \\ &+ \underbrace{Z_C^{\text{dia}}(\gamma - \Delta\gamma/2) - Z_C^{\text{dia}}(\gamma + \Delta\gamma/2) + \Delta Z_C^{\text{int}}}_{\text{particulate matter}}. \end{aligned} \quad 32.$$

Equation 32 is an evolution equation for tracer content decomposed into processes related to mass fluxes through the bounding surfaces plus those due to material tracer changes and, if relevant, the particulate matter through the bounding surfaces. This equation reveals that tracer budget studies are subject to ocean thermodynamics through the dianeutral transport component. **Figure 2** depicts the framework defined by Equation 32. It offers a framework from which to incorporate observational measures of relevant processes, such as air-sea fluxes, mixing, and biogeochemical sources.

It is notable that the formalism presented here can be applied over a variety of domains, from the ocean surface into the interior and to the bottom. For example, a central question in biogeochemistry concerns what sets a tracer distribution at some depth or density horizon within the ocean interior. Is the concentration set largely at the point of ventilation from the mixed layer, or is it determined more from interior processes, such as remineralization, respiration, or mixing? The budget terms shown in Equation 32 provide a flexible and robust framework to examine the various facets of this question.

#### 4.5. An Example Calculation for Nitrate

We consider the case of dissolved inorganic nitrate ( $\text{N}_i$ ) (Boyer et al. 2013) and its dianeutral transport from air-sea fluxes, small-scale buoyancy mixing, and mesoscale buoyancy mixing ( $F_{\text{N}_i}^{\text{bdy}}$ ,

**Figure 5**

(a,b) Inorganic nitrate ( $N_i$ ) distributions from *World Ocean Database 2013* (Boyer et al. 2013), with annual mean and maximum  $\gamma^n$  contours overlaid in black and white, respectively. (c,d) Dianutral  $N_i$  transports due to dianutral transport ( $E$  terms) and dianutral  $N_i$  diffusion ( $M$  terms) in Equation 32 for the Northern Hemisphere and the Southern Ocean, partitioned at 30°S. We here used the same data and diffusivities as for **Figure 4**. Similarly, mesoscale refers to the sum of neutral diffusion in the interior and horizontal diffusion in the boundary layer. Abbreviations: AABW, Antarctic Bottom Water; AAIW, Antarctic Intermediate Water; NACW, North Atlantic Central Water; NADW, North Atlantic Deep Water; SAMW, Subantarctic Mode Water.

$E_{N_i}^{\text{iso}}$ , and  $E_{N_i}^{\text{meso}}$ , respectively, with  $E_{N_i}^{\text{meso}} = E_{N_i}^{\text{hor}} + E_{N_i}^{\text{cab}} + E_{N_i}^{\text{tbl}}$ ). We also provide estimates of the dianutral tracer diffusion  $M_{N_i}^{\text{dia}}$ , split into small-scale and mesoscale components (**Figure 5c,d**). The magnitudes of the terms are of the same order as the total export of  $N_i$  from the photic zone (1,570 Tg N  $y^{-1}$ ) (Capone et al. 2008).

Biogeochemical processes transfer  $N_i$  toward dense waters due to sinking of particulate matter (Sarmiento & Gruber 2006). However, north of 30°S, a compensating transport of  $N_i$  of



**Subduction:** seawater mass transport from the surface to the interior through the mixed-layer base

**Ventilation:** tracer mass transport from the surface to the interior through the mixed-layer base

$\mathcal{O}(1,000 \text{ Tg N}_i \text{ y}^{-1})$  toward lighter water is observed. This transport is due to small-scale isotropic diffusion of heat and fresh water, leading to a diapycnal  $N_i$  transport (yellow line in **Figure 5c**). Simultaneously, surface buoyancy fluxes transport  $\mathcal{O}(500 \text{ Tg N}_i \text{ y}^{-1})$  toward both the lightest and densest waters (blue line in **Figure 5c**). Interestingly, at the base of the thermocline ( $\gamma^n \approx 25.5$ ), air-sea and diapycnal buoyancy fluxes and diapycnal  $N_i$  diffusion all promote an upwelling of  $N_i$  into lighter waters.

South of 30°S, diapycnal transport by mesoscale buoyancy fluxes leads to an accumulation of  $N_i$  of  $\mathcal{O}(1,500 \text{ Tg y}^{-1})$  in the range of  $\gamma^n = 28\text{--}28.5 \text{ kg m}^{-3}$  (orange line in **Figure 5d**), increasing the  $N_i$  content of Antarctic Bottom Water. Some of this Antarctic Bottom Water  $N_i$  is removed by small-scale mixing north of 30°S (yellow line in **Figure 5c**). It is possible that improved mixing estimates and/or biogeochemical processes not included here can account for additional removal of  $N_i$  from Antarctic Bottom Water. South of 30°S, dianutral  $N_i$  transport due to air-sea buoyancy fluxes leads to an accumulation of  $N_i$  in the Subantarctic Mode Water range, by transformation of Antarctic Intermediate Water and denser waters.  $N_i$  transport from Subtropical Mode Water to lighter waters related to equatorial upwelling supports primary production (blue line in **Figure 5c**). Although in general  $N_i$  diffusion is small, north of 30°S there is some diffusion of high  $N_i$  concentrations from the tongue (**Figure 4d**) to lighter waters by small-scale mixing (green line in **Figure 5c**).

We used constant diffusivities to generate **Figure 5**. Therefore, our analysis offers a simplified example of how WMT methods can be used to decompose  $N_i$  transports into individual physical and biogeochemical processes. Improved mixing estimates and air-sea  $N_i$  fluxes will offer a more accurate  $d(\Delta N_i)/dt$  budget analysis. We also conjecture that a WMT analysis could be useful to reconcile divergent views on the role of high latitudes in global primary production (Sarmiento et al. 2004, Holzer & Primeau 2013).

#### 4.6. Water Mass Transformation, Seawater Subduction, and Tracer Ventilation

Tracer ventilation was originally associated with transport of dissolved oxygen from the surface mixed layer to the interior, thus allowing for aerobic respiration in most of the oceanic layers. We now think of subduction (seawater transport) and ventilation (tracer transport)—concepts first introduced by Montgomery (1938) and Iselin (1939)—as the processes that move water, nutrients, and other tracers from the mixed layer into the interior.

**4.6.1. Mathematical formulation.** In general, water masses are renewed within ocean boundary layers, especially at the air-sea interface but also within the bottom boundary layer (Ferrari et al. 2016). The rate of injection of boundary-layer waters into the ocean interior is fundamental to the ocean's role in climate and biogeochemical cycles. Here, we focus on transport from the ocean mixed layer into the interior across the mixed-layer base. We show how processes affecting this transport are naturally studied using the WMT framework, thus allowing the methods of WMT analysis to be applied to subduction and ventilation studies.

To connect subduction and ventilation to the WMT framework, we consider the advective transport of tracer crossing the mixed-layer base within a neutral density layer. We write this boundary as  $\partial\Omega_{ml}(\gamma)$ , which is a special case of the boundary  $\partial\Omega_{int}$  shown in **Figure 3**. Likewise, the corresponding volume within the mixed layer is denoted  $\Omega_{ml}(\gamma)$ , which is the region within the  $\gamma$  layer above the mixed-layer base. Specializing the general expression in Equation 27, we write the advective transport of tracer across the mixed layer base as

$$\Delta\Psi_C^{ml}(\gamma) = \iint_{\partial\Omega_{ml}(\gamma)} \rho c (\mathbf{u} - \mathbf{u}_{ml}) \cdot \hat{\mathbf{n}}_{ml} dA. \quad 33.$$

21.20 Groeskamp et al.

Review in Advance first posted on September 19, 2018. (Changes may still occur before final publication.)



In this equation,  $\mathbf{u}_{\text{ml}}$  is the velocity of a point on the mixed-layer base, and  $\hat{\mathbf{n}}_{\text{ml}}$  is the unit normal pointing toward the ocean interior. Equation 33 defines the advective ventilation of a tracer. The special case of  $c = 1$  reduces the expression to subduction, written as  $\Delta\Psi^{\text{ml}}(\gamma)$ .

We can bring Equation 33 in line with the WMT formalism by defining a tracer that measures the depth relative to the mixed-layer base  $\lambda_{\text{ml}} \equiv -(z + b)$ ; here,  $-H \leq z \leq \eta$  is the range for  $z$  within the ocean, with  $z = -H(x, y)$  the ocean bottom,  $z = \eta(x, y, t)$  the ocean surface, and  $z = -b(x, y, t)$  the vertical position of the mixed-layer base. By construction, the mixed-layer base is the surface  $\lambda_{\text{ml}} = 0$ , whereas  $\lambda_{\text{ml}} < 0$  for regions within the mixed layer and  $\lambda_{\text{ml}} > 0$  for regions in the interior. The normal vector,  $\hat{\mathbf{n}}_{\text{ml}}$ , points toward regions of larger  $\lambda_{\text{ml}}$ , orienting flow so that positive subduction values are for water leaving the mixed layer moving into the interior [ $\Delta\Psi^{\text{ml}}(\gamma) < 0$  for obduction, the reverse process by which water returns to the mixed layer]. We write  $\lambda_{\text{ml}}(\gamma) = 0$  as the mixed-layer base within a particular  $\gamma$  layer. That is,  $\lambda_{\text{ml}}(\gamma) = 0$  is a particular representation of the boundary  $\partial\Omega_{\text{ml}}(\gamma)$ , and  $\lambda_{\text{ml}}(\gamma) < 0$  is a corresponding representation of the mixed-layer volume  $\Omega_{\text{ml}}(\gamma)$ . We can now make use of the WMT formalism from Section 2.2 to write

$$\Delta\Psi_C^{\text{ml}}(\gamma) = \iint_{\lambda(\gamma)=0} \frac{\rho c \dot{\lambda}' dA}{|\nabla \lambda|} = \frac{\partial}{\partial \lambda} \iiint_{\lambda'(\gamma) \leq 0} \rho c \dot{\lambda}' dV, \quad \lambda = \lambda_{\text{ml}} = -(b + z), \quad 34.$$

with  $\dot{\lambda}_{\text{ml}} = -(w + \partial_t b + \mathbf{u} \cdot \nabla b)$ . Note that  $\dot{\lambda}_{\text{ml}}$  is equivalent to the classical definition of instantaneous subduction at a point on the mixed-layer base (Cushman-Roisin 1987).

**4.6.2. Total ventilation and its potential application.** For some applications, it is useful to define an averaged tracer at the mixed-layer base  $\Delta\Psi_C^{\text{ml}}(\gamma) \equiv \bar{c} \Delta\Psi^{\text{ml}}(\gamma)$ , in which  $\bar{c}$  is the preformed tracer concentration (Broecker 1974) when considering biogeochemical tracers.

In addition to advective ventilation as defined by Equation 33, tracers are transported across the mixed-layer base via diffusion and particulate velocity. We thus define the net tracer ventilation as

$$\mathcal{S}_C \equiv \underbrace{\Delta\Psi_C^{\text{ml}}}_{\text{advective vent.}} + \underbrace{\Delta M_C^{\text{ml}}}_{\text{diffusive vent.}} + \underbrace{\Delta Z_C^{\text{ml}}}_{\text{particulate vent.}}, \quad 35.$$

where the diffusive  $\Delta M_C^{\text{ml}}$  and particulate velocity  $\Delta Z_C^{\text{ml}}$  terms are defined by applying Equations 28 and 31 to a mixed-layer base.

Subduction and ventilation are important quantities for climate dynamics, as they measure the exchange of properties between the upper ocean and the interior (Marshall et al. 1993, Sallée et al. 2010). Subduction requires estimates of the vertical velocity that are not available from observations, especially not on large spatial and long temporal scales. However, we can use the WMT formalism for ventilation in combination with the total budget represented by Equation 32 to obtain subduction and ventilation estimates from more readily available observations. We thus have a framework to study ventilation in the context of the suite of processes within the mixed layer and ocean surface, using either observations or numerical models. That is, Equation 32 quantifies the integral effect of processes that set the rate of tracer ventilation into the pycnocline, including export by sinking particles. It can also be applied to investigate heat, freshwater, and trace gas injection into the interior. Furthermore, coupling the kinematic definition with the WMT relates the thermodynamically based ventilation estimate (e.g., air-sea exchanges) to the residual mean advection.

## 5. A BRIEF HISTORICAL REVIEW

When Walin (1977, 1982) introduced the WMT framework, his key insight was to frame circulation in terms of moving layers rather than the stationary boxes that had been commonplace up to that time. This insight prompted many others to use the WMT framework to provide a



process-based decomposition of the water mass structure and circulation of the world ocean, showcasing the usefulness of the WMT framework as a tool to quantify and understand a wide variety of ocean phenomena. Here, we survey WMT studies from more than 40 years of WMT thinking and offer some insights for future applications to further understand the ocean and its role in the climate system.

### 5.1. Water Mass Transformation in Potential Density ( $\sigma$ ) Coordinates

Speer & Tziperman (1992) first derived the potential density ( $\sigma$ )-based WMT, as applied to surface forcing and mixing of water masses in the North Atlantic. This approach was extended in subsequent studies to infer diapycnal mixing from air-sea fluxes and advection in the North Atlantic (Speer 1998), interannual variations of the AMOC (Marsh 2000), the formation of dense Nordic Seas waters that feed the AMOC (Isachsen et al. 2007), geographical mapping of WMT patterns related to North Atlantic Subpolar Mode Water formation processes (Brambilla et al. 2008), seasonal and geographical details of North Atlantic Eighteen Degree Water formation (Maze et al. 2009), the role of air-sea buoyancy fluxes in the residual circulation in the Southern Ocean (Badin et al. 2010) and anomalous Subpolar Mode Water formation (Grist et al. 2016), and the dominant role of freshwater fluxes in the Southern Ocean overturning circulation (Pelichero et al. 2018).

Marshall et al. (1999) and Nurser et al. (1999) pioneered the use of  $\sigma$ -based WMT as a diagnostic to quantify the mixing processes in ocean circulation models. Subsequently, a series of model studies investigated topics such as Circumpolar Deep Water, Subantarctic Mode Water, and Antarctic Intermediate Water formation processes (Marsh et al. 2000); interannual to decadal variations in the transformation and overturning of North Atlantic water masses in an eddy-permitting model (Marsh et al. 2005); the role of cabbeling in the Southern Ocean in an eddy-resolving model (Urakawa & Hasumi 2012); Subantarctic Mode Water formation and destruction processes in the Southern Ocean State Estimate (SOSE) (Cerovecki et al. 2013); North Pacific Subtropical Mode Water formation processes (Nishikawa et al. 2013); multimodel ensemble AMOC streamfunctions (Danabasoglu et al. 2014, 2016); the role of sea-ice interaction and its seasonality (Abernathay et al. 2016); and topographic mixing in the Southern Ocean as diagnosed from SOSE (Tamsitt et al. 2018).

### 5.2. Water Mass Transformation in Neutral Density ( $\gamma^n$ ) Coordinates

A key improvement to  $\sigma$ -based WMT is the  $\gamma^n$ -based WMT pioneered by Iudicone et al. (2008b) in an analysis of a global ocean circulation model. Iudicone et al. (2008b) also emphasized the important role of warming below the mixed layer, driven by penetrative shortwave radiation for WMT and the overturning circulation. Processes affecting Southern Ocean overturning were described by Iudicone et al. (2008a), and carbon transports were examined by Iudicone et al. (2011). Groeskamp et al. (2016a) further applied the  $\gamma^n$  WMT framework to observations, thus highlighting the importance of cabbeling for Antarctic Intermediate Water formation. Groeskamp & Iudicone (2018) showed the importance of chlorophyll *a* for circulation and mixing due to its influence on both the albedo and the penetration of shortwave radiation.

### 5.3. Water Mass Transformation in $\Theta$ , $S_A$ , and $\Theta$ and $S_A$ Coordinates

One-dimensional circulation in buoyancy coordinates can be decomposed into two dimensions by separately quantifying the contribution from  $\Theta$  or  $S_A$  changes (Speer 1993). WMT in  $\Theta$  and  $S_A$  coordinates is more fundamental since  $\Theta$  and  $S_A$  are conservative scalar properties, but the link with observed circulation is less straightforward. Nonetheless, it is conceptually natural to

view the ocean's thermohaline circulation using thermohaline coordinates, as first achieved by Döös et al. (2012), Zika et al. (2012), and Groeskamp et al. (2014a). Doing so allows one to study processes directly affecting the circulation (Hieronymus et al. 2014). Evans et al. (2014) used WMT in  $\Theta$  and  $S_A$  coordinates to reveal the importance of a seasonal interplay between air-sea and diffusive buoyancy fluxes for Antarctic Intermediate Water, Circumpolar Deep Water, and Antarctic Winter Water formation in the Drake Passage, and Pemberton et al. (2015) quantified WMT related to water circulating into and out of the Arctic basin. Zika et al. (2015), Grist et al. (2016), and Skliris et al. (2016, 2018) used WMT in just  $S_A$  coordinates to quantify hydrological cycle change. Evans et al. (2017) used WMT in  $\Theta$  coordinates (as in Walin 1982) to reconcile observed wind-driven changes in the AMOC at 26°N with observed changes in water masses.

#### 5.4. Water Mass Transformation and Biogeochemistry

Only a few studies have actually combined the WMT framework with biogeochemistry. Iudicone et al. (2011) pioneered the use of WMT to study biogeochemical tracer transport (Section 4), and in so doing provided a process-based understanding of how the Southern Ocean overturning affects carbon uptake and the resulting export to the world ocean. Groeskamp et al. (2016b), Iudicone et al. (2016), and Zhai et al. (2017) further investigated uptake, transport, and storage pathways of (anthropogenic) carbon using a WMT process-based decomposition. Badin et al. (2010) combined the  $\sigma$ -based WMT framework with nutrient concentrations to connect biological consumption to air-sea and diffusive buoyancy fluxes.

The combination of the WMT framework with biogeochemistry, as given by Equation 32, relates physical processes (circulation and mixing) and biological processes (functional gene expressions, biotic interactions, etc.). In Section 6, we further detail our view on the benefits of combining WMT and biogeochemistry. Motivated by recent studies, we here highlight potential applications of Equation 32 for determining key processes regulating ocean biogeochemistry, such as regulating the biogeography of the oceans (Coles et al. 2017) and their response to climate change (Boyd et al. 2015), and for providing a process-based decomposition of ventilation and subduction (MacGilchrist et al. 2017, Buongiorno Nardelli et al. 2018).

#### 5.5. Water Mass Transformation and Inverse Methods

The ocean circulation is forced primarily by large-scale processes (winds and tides) and dissipated by small-scale turbulent mixing (Section 3.3). Key advances in oceanography are expected to come from understanding the coupling between small-scale processes and the large-scale circulation and climate (Garabato 2012, MacKinnon et al. 2013). The WMT framework encompasses this coupling by combining observations of the ocean's  $\Theta$  and  $S_A$  structure to estimates of boundary buoyancy fluxes and physical processes.

Buoyancy-based WMT studies, combined with box-inverse methods (Wunsch 1978), have proven useful to estimate diapycnal transports and reveal the importance of air-sea fluxes for the Southern Ocean overturning circulation (Sloyan & Rintoul 2001), topographically induced mixing for bottom water export (Naveira Garabato et al. 2003), mixing in Nordic Seas overturning (Isachsen & Nøst 2012), and the epineutral and dianeutral North Pacific circulation (Hautala 2018). The thermohaline inverse method of Groeskamp et al. (2014b, 2017) utilized the readily available hydrographic  $\Theta$  and  $S_A$  data and estimates of air-sea fluxes to infer the circulation in  $\Theta$  and  $S_A$  coordinates. These studies also quantified the spatial distribution of small-scale and mesoscale turbulent processes. A recent study by Mackay et al. (2018) merged both the  $\Theta$  and  $S_A$  method of Groeskamp et al. (2014b) and the box-inverse method, demonstrating how ongoing advances in WMT are being used to enhance ship-based observational programs.



## 6. THE KEY ROLE FOR WATER MASS TRANSFORMATION ANALYSIS IN FUTURE CLIMATE AND ECOSYSTEM STUDIES

The ocean's role in climate and ecosystems largely involves combined effects of subduction of water masses, the overturning circulation, and ventilation of thermodynamic, chemical, and biogeochemical properties. Accurate quantification and simulation of these phenomena and their drivers are essential to understanding past and future climate and ecosystem changes on global to regional scales. The WMT framework builds from the intimate connections among ocean dynamics, thermodynamics, biogeochemical processes, and air-sea, ice-sea, and earth-sea interactions. Consequently, a WMT framework provides a natural means to obtain a process-based understanding and quantification of ocean and tracer circulation.

Directly quantifying ocean and tracer circulation over large spatial and temporal scales is limited by logistical and technological challenges, most notably in remote and hostile environments such as the Southern Ocean. However, with autonomous observations [from Argo floats, the Southern Ocean Carbon and Climate Observations and Modeling (SOCCOM) program, and gliders], novel satellite measurements [from the Soil Moisture and Ocean Salinity (SMOS) satellite], and the GEOTRACES program, large-scale distributions of variables such as  $S$ ,  $\Theta$ , and  $N$ , are now readily available, alongside local observations of key fine-scale processes (e.g., small-scale mixing and air-sea fluxes). Improvements in space-time coverage and the enhanced fidelity of observational sampling offer compelling reasons to work within the conceptual and quantitative framework of Equation 32.

Many terms in Equation 32 can be, or soon will be, obtained from observations with suitable accuracy, providing an unparalleled opportunity to understand ocean tracer circulation according to an observation-based process perspective. With the WMT framework, perhaps combined with inverse methods, we can quantify fine-scale processes through inferences based on the measured large scale and vice versa, depending on which variables are more readily measured. The WMT framework thus provides a fruitful means to answer basic and critical questions related to processes and their evolution. This perspective in turn offers an independent means to evaluate numerical ocean circulation and biogeochemical models. We therefore propose that the WMT framework is key to furthering scientific progress in quantifying and conceptualizing changes in Earth's climate and ecosystems.

## 7. APPENDIX 1: MATHEMATICAL FOUNDATIONS

The mathematical foundation of the WMT framework relies on the existence of smooth scalar fields, thus allowing for the use of calculus (i.e., integration and differentiation) to perform budget analyses within a layer bounded by  $\lambda$  iso-surfaces. We are generally afforded smooth tracer surfaces at space-time scales larger than the microscale (millimeters and seconds; see figure 2 of McWilliams 1998). The presentation given here is motivated by Marshall et al. (1999, 2006); it differs from the earlier formalism of Walin (1982) and Nurser et al. (1999), but the resulting budget equations are equivalent.

### 7.1. Translating $u^{\text{dia}}$ into $\dot{\lambda}$

A key to formulating the equations of WMT is to connect  $u^{\text{dia}}$  to material changes in  $\lambda$ :

$$\dot{\lambda} = \frac{\partial \lambda}{\partial t} + \mathbf{u} \cdot \nabla \lambda. \quad 36.$$

21.24 Groeskamp et al.

 Review in Advance first posted on September 19, 2018. (Changes may still occur before final publication.)

To do so, write the differential increment  $d\lambda(\mathbf{x}, t)$  in terms of its space and time changes:

$$d\lambda = d\mathbf{x} \cdot \nabla\lambda + dt \frac{\partial\lambda}{\partial t}. \quad 37.$$

By construction, a point fixed on a moving  $\lambda$  surface maintains fixed  $\lambda$  ( $d\lambda = 0$ ) so that

$$\frac{d\mathbf{x}_\lambda}{dt} \cdot \nabla\lambda \equiv \mathbf{u}_\lambda \cdot \nabla\lambda = -\frac{\partial\lambda}{\partial t}. \quad 38.$$

Hence, when following a moving  $\lambda$  iso-surface, changes in space are precisely compensated by changes in time. Inserting Equation 38 into Equation 1 leads to

$$u^{\text{dia}} \equiv \mathbf{u} \cdot \hat{\mathbf{n}}_\lambda + \frac{1}{|\nabla\lambda|} \frac{\partial\lambda}{\partial t} = \frac{\dot{\lambda}}{|\nabla\lambda|}. \quad 39.$$

## 7.2. Volume Integration

Consider a cylinder extending between the two  $\lambda$  iso-surfaces with volume  $\delta V = \delta A \delta b$ , where  $\delta A$  is the cross-sectional area and  $\delta b$  the thickness. Both the area and the thickness are oriented according to the normal vector  $\hat{\mathbf{n}}_\lambda = |\nabla\lambda|^{-1} \nabla\lambda$ . Consequently, the thickness is related to the differential tracer increment according to  $d\lambda = \nabla\lambda \cdot d\mathbf{x} = |\nabla\lambda| \hat{\mathbf{n}}_\lambda \cdot d\mathbf{x} = |\nabla\lambda| \delta b$ , leading to the cylinder volume  $\delta V = |\nabla\lambda|^{-1} \delta A \delta\lambda$ .

Now consider the volume of a cylinder extending from the lower bound of the  $\lambda$  range, written as  $\lambda_0$ , to an arbitrary value of  $\lambda$ :

$$V(\lambda) = \iiint_{\lambda_0 \leq \lambda} dV = \int_{\lambda_0}^{\lambda} d\lambda' \iint \frac{dA}{|\nabla\lambda'|}, \quad 40.$$

where we used  $dV = |\nabla\lambda|^{-1} d\lambda dA$  to reach the second equality (assuming  $|\nabla\lambda| \neq 0$ ). The volume is inversely proportional to the magnitude of the tracer gradient so that regions of strong gradients have relatively small volumes. The volume integration between the two tracer surfaces is valid even if the surfaces are not monotonic in any particular direction. For example, overturning surfaces are allowed, as are surfaces enclosing isolated fluid regions (Figure 3).

We generally assume that the lower integration limit in Equation 40 is an arbitrary value below the range of  $\lambda$  found in the ocean, so that  $V(\lambda)$  measures the volume of all seawater beneath an arbitrary  $\lambda$  surface. Consequently, the volume of a shell region between two  $\lambda$  surfaces separated by  $\Delta\lambda/2$  is given by the finite difference expression

$$\Delta V(\lambda) = V(\lambda + \Delta\lambda/2) - V(\lambda - \Delta\lambda/2) = \int_{\lambda - \Delta\lambda/2}^{\lambda + \Delta\lambda/2} d\lambda' \iint \frac{dA}{|\nabla\lambda'|}. \quad 41.$$

Notice how the arbitrary reference value,  $\lambda_0$ , drops out from this expression for the layer volume. We can make use of this identity for the volume integral of an arbitrary function over a  $\lambda$  layer.

## 7.3. Area Integration

We now consider an arbitrary function integrated over a surface bounded by two  $\lambda$  values. Particular cases are the ocean surface boundary,  $\partial\Omega_{\text{out}}(\lambda)$ , and an interior boundary,  $\partial\Omega_{\text{int}}(\lambda)$  (see Figure 3). In the general case with a lower bound of  $\lambda_0$ , the area integral takes on the form  $\Sigma(\lambda) = \iint_{\lambda_0}^{\lambda} \sigma dA$ , so that the area integral over the boundary of a layer [say,  $\partial\Omega_{\text{int}}(\lambda)$ ] in



Review in Advance first posted on  
September 19, 2018. (Changes may  
still occur before final publication.)

**Figure 3]** is

$$\Delta\Sigma = \Sigma(\lambda + \Delta\lambda/2) - \Sigma(\lambda - \Delta\lambda/2) = \iint_{\partial\Omega_{\text{int}}(\lambda)} \sigma \, dA = \iint_{\lambda - \Delta\lambda/2}^{\lambda + \Delta\lambda/2} \sigma \, dA. \quad 42.$$

#### 7.4. Using the Fundamental Theorem of Calculus

For an integral  $H = \int_{\lambda_0}^{\lambda} \mathcal{H}(\lambda') \, d\lambda'$ , the fundamental theorem of calculus says that  $\partial H / \partial \lambda = \mathcal{H}(\lambda)$ . From Equation 40, the fundamental theorem of calculus leads to the identity

$$\frac{\partial V(\lambda)}{\partial \lambda} = \iint_{\lambda} \frac{dA}{|\nabla \lambda|}. \quad 43.$$

Notably, this identity also holds for the integral of an arbitrary function over the volume. In particular, the dia-surface transport written in the form of an area integral as in Equation 3 can be written

$$G(\lambda) = \iint_{\lambda} \frac{\rho \dot{\lambda} \, dA}{|\nabla \lambda|} = \frac{\partial}{\partial \lambda} \iint_{\lambda' \leq \lambda} \rho \dot{\lambda}' \, dV. \quad 44.$$

This identity is of great practical value for the WMT formalism since the volume integral is simpler to compute with discrete data than the area integral.

#### 7.5. Discrete Approximations

The derivative operator acting on the volume integral in Equation 43 can be approximated by the centered difference expression

$$\frac{\partial V}{\partial \lambda} \approx \frac{\Delta V}{\Delta \lambda} = \frac{V(\lambda + \Delta\lambda/2) - V(\lambda - \Delta\lambda/2)}{\Delta\lambda} = \frac{1}{\Delta\lambda} \int_{\lambda - \Delta\lambda/2}^{\lambda + \Delta\lambda/2} d\lambda' \iint \frac{dA}{|\nabla \lambda'|}. \quad 45.$$

We can provide a discrete approximation of this volume integral over a layer  $\lambda \in [\lambda - \Delta\lambda/2, \lambda + \Delta\lambda/2]$  by introducing a boxcar function (e.g., Brambilla et al. 2008, Iudicone et al. 2008b, Maze et al. 2009, Badin et al. 2010):

$$\Pi(\lambda_n, \lambda, \Delta\lambda) = \begin{cases} 1 & \text{if } \lambda_n \in [\lambda - \Delta\lambda/2, \lambda + \Delta\lambda/2] \\ 0 & \text{otherwise.} \end{cases} \quad 46.$$

The index  $n \in [0, N]$  is an integer, with  $\lambda_n = \lambda_0 + n \Delta\lambda$  a discrete partitioning of  $\lambda$  over its range. We thus have the discrete estimate

$$\frac{\partial V}{\partial \lambda} \approx \frac{1}{\Delta\lambda} \sum_n \sum_{i,j,k} \Pi(\lambda_n, \lambda, \Delta\lambda) V_{i,j,k}, \quad 47.$$

where  $V_{i,j,k}$  is the grid cell volume labeled by the integers  $i, j, k$ . These considerations also hold when including an arbitrary function, such as the WMT as written in Equation 44,

$$G(\lambda) \approx \frac{1}{\Delta\lambda} \sum_n \sum_{i,j,k} \Pi(\lambda_n, \lambda, \Delta\lambda) (\rho \dot{\lambda})_{i,j,k} V_{i,j,k}, \quad 48.$$

or when  $(\rho \dot{\lambda})$  is replaced with  $(\rho c \dot{\lambda})$  for calculations of  $E_C$  terms from Equation 25b.



## 8. APPENDIX 2: THE EVOLUTION OF LOCALLY REFERENCED POTENTIAL DENSITY

The material time evolution of locally referenced potential density is

$$\dot{\rho}_l = \rho(-\alpha \dot{\Theta} + \beta \dot{S}). \quad 49.$$

To isolate physical processes affecting density, we follow Iudicone et al. (2008b) by decomposing the material evolution of salinity and temperature into boundary contributions (including penetrative shortwave radiation) and interior mixing contributions.

### 8.1. Salinity

The material evolution of salinity can be written as

$$\rho \dot{S} = -\nabla \cdot \mathbf{J}_S + \underbrace{[F_S + Q_m(S_m - S)]}_{\text{boundary salinity flux}} \delta(z - \eta). \quad 50.$$

The first term,  $-\nabla \cdot \mathbf{J}_S$ , arises from the convergence of interior mixing processes such as down-gradient diffusion (see Section 8.3). The second term,  $F_S$ , arises from exchanges of salt and fresh water across the ocean boundary, e.g., sea-ice interactions or salinity damping, as applied in some numerical models. The third term arises from the transfer of mass across the boundary, with  $Q_m$  the boundary mass flux ( $Q_m > 0$  for mass entering the ocean). Additionally,  $S_m - S$  is the difference between the salinity contained in the total transferred mass (e.g., salty estuarine inflow) and the sea surface salinity. Note that none of these three terms involve any associated mass tendency; they represent convergences of salinity fluxes, i.e., fluxes of salt one way balanced by opposite fluxes of fresh water. The Dirac delta,  $\delta(z - \eta)$ , is nonzero only at the ocean surface,  $z = \eta(x, y, t)$ . It picks out one portion of a vertical convergence at the surface boundary and so carries dimensions of inverse length.

### 8.2. Conservative Temperature

The material evolution of Conservative Temperature is the sum of various terms ( $\text{W m}^{-3}$ ):

$$C_p \rho \dot{\Theta} = -\nabla \cdot \mathbf{J}_Q - \nabla \cdot \mathbf{J}_Q^{\text{short}} + [F_Q + C_p Q_m (\Theta_m - \Theta)] \delta(z - \eta) + F_{\text{geo}} \delta(z + H), \quad 51.$$

where  $C_p$  is the seawater heat capacity ( $\text{J kg}^{-1} \text{K}^{-1}$ ). The first term,  $-\nabla \cdot \mathbf{J}_Q$ , arises from the convergence of interior mixing processes, whereas the second term,  $-\nabla \cdot \mathbf{J}_Q^{\text{short}}$ , arises from the convergence of penetrative shortwave radiation.  $F_Q$  encompasses surface boundary heating from turbulent and radiative (other than shortwave) contributions.  $C_p Q_m (\Theta_m - \Theta)$  accounts for the heat content of mass transferred across the ocean boundary, with  $\Theta_m$  the Conservative Temperature of the mass flux. Finally,  $F_{\text{geo}}$  arises from bottom geothermal heating at  $z = -H(x, y)$ . The surface and geothermal fluxes are positive for heat added to the ocean domain.

### 8.3. Impacts of Diffusion on Locally Referenced Potential Density

Here, we identify how diffusion affects the material evolution of locally referenced potential density, whereby

$$(\dot{\rho}_l)_{\text{diffusion}} = \alpha \nabla \cdot \mathbf{J}_{\Theta} - \beta \nabla \cdot \mathbf{J}_S. \quad 52.$$



The diffusive fluxes for salinity and temperature can be written as

$$\mathbf{J}_S = -\rho \mathbf{K} \cdot \nabla S, \quad \mathbf{J}_\Theta = -\rho \mathbf{K} \cdot \nabla \Theta, \quad 53.$$

where  $\mathbf{K}$  is a symmetric positive-definite kinematic diffusivity tensor ( $\text{m}^2 \text{ s}^{-1}$ ). The minus sign arises from the downgradient nature of the diffusive flux.  $\mathbf{K}$  is written as the sum of mesoscale neutral diffusion, horizontal diffusion, and small-scale isotropic diffusion (Section 3.3):

$$\mathbf{K} = K_N (\mathbf{I} - \hat{\mathbf{n}}_\rho \hat{\mathbf{n}}_\rho) + K_H (\mathbf{I} - \hat{\mathbf{z}} \hat{\mathbf{z}}) + D \mathbf{I}. \quad 54.$$

Here,  $\mathbf{I}$  is the identity tensor;  $\hat{\mathbf{z}} = (0, 0, 1)$  is the vertical unit vector;  $K_N > 0$ ,  $K_H > 0$ , and  $D > 0$  are the neutral, horizontal, and isotropic eddy diffusivities; and the dianeutral unit vector  $\hat{\mathbf{n}}_\rho$  is defined by Equation 11. The material evolution of density arising from diffusion is thus given by

$$(\dot{\rho}_l)_{\text{diff}} = \underbrace{\alpha \nabla \cdot \mathbf{J}_\Theta^{\text{ntr}} - \beta \nabla \cdot \mathbf{J}_S^{\text{ntr}}}_{\text{neutral diffusion } (\dot{\rho})_{\text{ntr}}} + \underbrace{\alpha \nabla \cdot \mathbf{J}_\Theta^{\text{iso}} - \beta \nabla \cdot \mathbf{J}_S^{\text{iso}}}_{\text{isotropic diffusion } (\dot{\rho})_{\text{iso}}} + \underbrace{\alpha \nabla \cdot \mathbf{J}_\Theta^{\text{hor}} - \beta \nabla \cdot \mathbf{J}_S^{\text{hor}}}_{\text{horizontal diffusion } (\dot{\rho})_{\text{hor}}}. \quad 55.$$

By construction, the neutral diffusive fluxes of temperature and salinity exactly compensate so that  $-\alpha \mathbf{J}_\Theta^{\text{ntr}} + \beta \mathbf{J}_S^{\text{ntr}} = 0$ , thus leading to (McDougall 1987b)

$$(\dot{\rho}_l)_{\text{ntr}} = \alpha \nabla \cdot \mathbf{J}_\Theta^{\text{ntr}} - \beta \nabla \cdot \mathbf{J}_S^{\text{ntr}} = \underbrace{\rho K_N C_b |\nabla_N \Theta|^2}_{\text{cabbeling (Cab)}} + \underbrace{\rho K_N T_b \nabla_N P \cdot \nabla_N \Theta}_{\text{thermobaricity (Thb)}}, \quad 56.$$

where

$$\nabla_N \Theta = \nabla \Theta - \hat{\mathbf{n}}_\rho (\hat{\mathbf{n}}_\rho \cdot \nabla \Theta). \quad 57.$$

The first term in Equation 56 is called cabbeling (Foster 1972), and the second is thermobaricity (McDougall 1987b). Their respective cabbeling and thermobaricity coefficients,  $C_b = C_b(S, \Theta, P)$  and  $T_b = T_b(S, \Theta, P)$ , are nonzero only due to nonlinearities in the equation of state.

## 9. APPENDIX 3: TRACER BUDGETS IN THE WATER MASS TRANSFORMATION FRAMEWORK

Let  $c$  be the concentration of a trace constituent, given by the ratio of the tracer mass to seawater mass (e.g.,  $\text{g kg}^{-1}$ , as for  $S_A$ ). Correspondingly, let  $\Delta C$  be the tracer mass within an arbitrary domain  $\Omega$ :

$$\Delta C = \iiint_{\Omega} \rho c \, dV. \quad 58.$$

The evolution of  $\Delta C$  depends on the evolution of the domain itself as well as the material evolution of  $c$ . We can formulate an evolution equation by making use of the Leibniz–Reynolds transport theorem:

$$\frac{d(\Delta C)}{dt} = \iiint_{\Omega} \frac{\partial(\rho c)}{\partial t} \, dV + \iint_{\partial\Omega} \rho c \mathbf{u}_b \cdot \hat{\mathbf{n}}_b \, dA, \quad 59.$$

where  $\mathbf{u}_b$  is the velocity of a point on the domain boundary,  $\partial\Omega$ , and  $\hat{\mathbf{n}}_b$  is the outward normal. We eliminate the local time tendency through use of the tracer equation

$$\rho \dot{c} = \frac{\partial(\rho c)}{\partial t} + \nabla \cdot (\rho c \mathbf{u}). \quad 60.$$

Integrating over the domain and using Gauss's law renders

$$\frac{d(\Delta C)}{dt} = \iiint_{\Omega} \rho \dot{c} \, dV - \iint_{\partial\Omega} \rho c (\mathbf{u} - \mathbf{u}_b) \cdot \hat{\mathbf{n}}_b \, dA. \quad 61.$$

Equation 61 is used throughout our discussion of tracer budgets in Section 4.



## 10. APPENDIX 4: CONCERNING DISCRETIZATION AND SAMPLING

Here, we consider certain practical issues that arise when performing WMT analysis using either observation-based or model-based data.

### 10.1. Coarse Vertical Casts Can Create Noisy Water Mass Transformation

The resolution of the bins used to compute the WMT (temperature, density, etc.) often exceeds the vertical resolution of a cast, particularly in a model. Sharp vertical gradients (e.g., a tropical thermocline) can be left with relatively few grid points representing gradients, potentially leading to a noisy WMT analysis. One approach to remedy the noise is to attempt to refine the resolution of the vertical cast by interpolation. However, interpolation is only as good as the underlying information provided, so it should be handled carefully to avoid spurious results.

### 10.2. Noise from the Tendency Term

A WMT analysis relies on estimates of tendency terms. Noise (i.e., enhanced power at the grid scale) in these terms can be amplified by the WMT analysis. For example, in numerical simulations, the diffusion operator acts to smooth property gradients. Hence, the diffusion tendency itself can be noisy, with this noise also reflected in the WMT.

### 10.3. Offline Versus Online Diagnostics

WMT is most accurately calculated when diagnosing tendency terms directly within the model simulation at each model time step. Absent such complete diagnostics, it is tempting to use offline approximations. However, we strongly caution against this approach, as it is very difficult to ensure budget closures using recomputed tendency terms. Additionally, transients lead to nonzero correlations that can be absent from an offline analysis.

### 10.4. Concerning Spurious Mixing

Discretization of the advection operator can cause significant (unrealistic) spurious mixing (Griffies et al. 2000). Practitioners generally aim to reduce the spurious mixing. However, properly accounting for spurious mixing in WMT analysis remains a conceptual and technical problem with no community consensus. The WMT framework may offer means to quantify spurious mixing as a residual of all transformation terms that can be explicitly diagnosed within a numerical model (e.g., Lee et al. 2002, Megann 2018).

## DISCLOSURE STATEMENT

The authors are not aware of any affiliations, memberships, funding, or financial holdings that might be perceived as affecting the objectivity of this review.

## ACKNOWLEDGMENTS

This review benefited from fruitful collaborations with numerous colleagues whose insights helped to inform our understanding of WMT analysis, ocean circulation, physical processes, and biogeochemistry. We thank illustrator Malou Zuidema for creating **Figure 2**. We thank Emily Newsom,



Ryan Holmes, Ivy Frenger, Keith Rodgers, and Graeme MacGilchrist for their valuable comments and suggestions on early drafts. S.M.G. thanks the National Oceanic and Atmospheric Administration's Geophysical Fluid Dynamics Laboratory for ongoing support and for providing a nurturing and stimulating research environment. S.G. thanks Trevor McDougall for being a great mentor over the past years and for providing the resources to pursue this work.

## LITERATURE CITED

- Abernathay RP, Cerovecki I, Holland PR, Newsom E, Mazloff M, Talley LD. 2016. Water-mass transformation by sea ice in the upper branch of the Southern Ocean overturning. *Nat. Geosci.* 9:596–601
- Abernathay RP, Marshall J. 2013. Global surface eddy diffusivities derived from satellite altimetry. *J. Geophys. Res. Oceans* 118:901–16
- Aumont O, Éthé C, Tagliabue A, Bopp L, Gehlen M. 2015. PISCES-v2: an ocean biogeochemical model for carbon and ecosystem studies. *Geosci. Model. Dev.* 8:2465–513
- Badin G, Williams RG, Sharples J. 2010. Water-mass transformation in the shelf seas. *J. Mar. Res.* 68:189–214
- Boyd PW, Lennartz ST, Glover DM, Doney SC. 2015. Biological ramifications of climate-change-mediated oceanic multi-stressors. *Nat. Clim. Change* 5:71–79
- Boyer T, Antonov JI, Baranova OK, Coleman C, Garcia HE, et al. 2013. *World Ocean Database 2013*. ed. S Levitus, tech. ed. A Mishonov. NOAA Atlas NESDIS 72. Silver Spring, MD: Natl. Ocean. Atmos. Adm. <http://doi.org/10.7289/V5NZ85MT>
- Brambilla E, Talley LD, Robbins PE. 2008. Subpolar mode water in the northeastern Atlantic: 2. Origin and transformation. *J. Geophys. Res. Oceans* 113:C04026
- Broecker WS. 1974. “NO”, a conservative water-mass tracer. *Earth Planet. Sci. Lett.* 23:100–7
- Broecker WS. 1982. *Tracers in the Sea*. Palisades, NY: Eldigio
- Buongiorno Nardelli B, Mulet S, Iudicone D. 2018. Three-dimensional ageostrophic motion and water mass subduction in the Southern Ocean. *J. Geophys. Res. Oceans* 123:1533–62
- Capone DG, Bronk DA, Mulholland MR, Carpenter EJ. 2008. *Nitrogen in the Marine Environment*. Burlington, MA: Academic. 2nd ed.
- Cerovecki I, Talley LD, Mazloff MR, Maze G. 2013. Subantarctic Mode Water formation, destruction, and export in the eddy-permitting Southern Ocean state estimate. *J. Phys. Oceanogr.* 43:1485–511
- Cole ST, Wortham C, Kunze E, Owens WB. 2015. Eddy stirring and horizontal diffusivity from Argo float observations: geographic and depth variability. *Geophys. Res. Lett.* 42:3989–97
- Coles VJ, Stukel MR, Brooks MT, Burd A, Crump BC, et al. 2017. Ocean biogeochemistry modeled with emergent trait-based genomics. *Science* 358:1149–54
- Cushman-Roisin B. 1987. Subduction. In *Dynamics of the Oceanic Surface Mixed Layer*, ed. P Muller, D Henderson, pp. 181–96. Honolulu: Hawaii Inst. Geophys.
- Danabasoglu G, Yeager SG, Bailey D, Behrens E, Bentsen M, et al. 2014. North Atlantic simulations in Coordinated Ocean-ice Reference Experiments phase II (CORE-II). Part I: mean states. *Ocean Model.* 73:76–107
- Danabasoglu G, Yeager SG, Kim WM, Behrens E, Bentsen M, et al. 2016. North Atlantic simulations in Coordinated Ocean-ice Reference Experiments phase II (CORE-II). Part II: inter-annual to decadal variability. *Ocean Model.* 97:65–90
- de Lavergne C, Madec G, Le Sommer J, Nurser AJG, Naveira Garabato AC. 2015. On the consumption of Antarctic Bottom Water in the abyssal ocean. *J. Phys. Oceanogr.* 46:635–61
- Defant A. 1936. Die Troposphäre. In *Wissenschaftliche Ergebnisse der Deutschen Atlantischen Expedition auf dem Forschungs- und Vermessungsschiff “Meteor”*, Vol. 6: *Schichtung und Zirkulation des Atlantischen Ozeans*, by G Wüst, A Defant, pp. 289–411. Berlin: Walter de Gruyter
- Döös K, Kjellsson J, Zika J, Laliberté F, Brodeau L, Aldama Campino A. 2016. The coupled ocean-atmosphere hydrothermohaline circulation. *J. Clim.* 30:631–47
- Döös K, Nilsson J, Nycander J, Brodeau L, Ballarotta M. 2012. The world ocean thermohaline circulation. *J. Phys. Oceanogr.* 42:1445–60



- Döös K, Webb DJ. 1994. The Deacon cell and the other meridional cells of the Southern Ocean. *J. Phys. Oceanogr.* 24:429–42
- Eckart C. 1948. An analysis of the stirring and mixing processes in incompressible fluids. *J. Mar. Res.* 7:265–75
- Einstein A. 1905. Über die von der molekularkinetischen Theorie der Wärme geforderte Bewegung von in ruhenden Flüssigkeiten suspendierten Teilchen. *Ann. Phys.* 322:549–60
- Ellis H. 1751. A letter to the Rev. Dr. Hales, F.R.S. from Captain Henry Ellis, F.R.S. *Philos. Trans. R. Soc. Lond.* 47:211–16
- Evans DG, Toole J, Forget G, Zika JD, Garabato ACN, et al. 2017. Recent wind-driven variability in Atlantic water mass distribution and meridional overturning circulation. *J. Phys. Oceanogr.* 47:633–47
- Evans DG, Zika JD, Garabato ACN, Nurser AJG. 2014. The imprint of Southern Ocean overturning on seasonal water mass variability in drake passage. *J. Geophys. Res. Oceans* 119:7987–8010
- Farneti R, Downes SM, Griffies SM, Marsland SJ, Behrens E, et al. 2015. An assessment of Antarctic Circumpolar Current and Southern Ocean meridional overturning circulation during 1958–2007 in a suite of interannual CORE-II simulations. *Ocean Model.* 94:84–120
- Ferrari R, Ferreira D. 2011. What processes drive the ocean heat transport? *Ocean Model.* 38:171–86
- Ferrari R, Mashayek A, McDougall T, Nikurashin M, Campin JM. 2016. Turning ocean mixing upside down. *J. Phys. Oceanogr.* 46:2239–61
- Ferrari R, McWilliams JC, Canuto VM, Dubovikov M. 2008. Parameterization of eddy fluxes near oceanic boundaries. *J. Clim.* 21:2770–89
- Foster TD. 1972. An analysis of the cabbeling instability in sea water. *J. Phys. Oceanogr.* 2:294–301
- Ganachaud A, Wunsch C. 2000. Improved estimates of global ocean circulation, heat transport and mixing from hydrographic data. *Nature* 408:453–57
- Garabato ACN. 2012. A perspective on the future of physical oceanography. *Philos. Trans. R. Soc. A* 370:5480–511
- Garrett C. 2001. Stirring and mixing: What are the rate-controlling processes? In *From Stirring to Mixing in a Stratified Ocean: Proceedings of the Twelfth 'Aba Huliko'a Hawaiian Winter Workshop*, pp. 1–8. Honolulu: Univ. Hawaii
- Gent PR, Willebrand J, McDougall TJ, McWilliams JC. 1995. Parameterizing eddy-induced tracer transports in ocean circulation models. *J. Phys. Oceanogr.* 25:463–74
- Gill AE. 1982. *Atmosphere-Ocean Dynamics*. San Diego, CA: Academic
- Gnanadesikan A, Anderson WG. 2009. Ocean water clarity and the ocean general circulation in a coupled climate model. *J. Phys. Oceanogr.* 39:314–32
- Graham FS, McDougall TJ. 2013. Quantifying the nonconservative production of Conservative Temperature, potential temperature, and entropy. *J. Phys. Oceanogr.* 43:838–62
- Griffies SM. 2004. *Fundamentals of Ocean Climate Models*. Princeton, NJ: Princeton Univ. Press
- Griffies SM, Gnanadesikan A, Pacanowski RC, Larichev V, Dukowicz JK, Smith RD. 1998. Isoneutral diffusion in a  $z$ -coordinate ocean model. *J. Phys. Oceanogr.* 28:805–30
- Griffies SM, Pacanowski RC, Hallberg RW. 2000. Spurious diapycnal mixing associated with advection in a  $z$ -coordinate ocean model. *Mon. Weather Rev.* 128:538–64
- Grist JP, Josey SA, Jacobs ZL, Marsh R, Sinha B, Van Sebille E. 2016. Extreme air-sea interaction over the North Atlantic subpolar gyre during the winter of 2013–2014 and its sub-surface legacy. *Clim. Dyn.* 46:4027–45
- Groeskamp S, Abernathey RP, Klocker A. 2016a. Water mass transformation by cabbeling and thermobaricity. *Geophys. Res. Lett.* 43:10835–45
- Groeskamp S, Iudicone D. 2018. The effect of air-sea flux products, short wave radiation depth penetration and albedo on the upper ocean overturning circulation. *Geophys. Res. Lett.* In press. <https://doi.org/10.1029/2018GL078442>
- Groeskamp S, Lenton A, Matear R, Sloyan BM, Langlais C. 2016b. Anthropogenic carbon in the ocean—surface to interior connections. *Glob. Biogeochem. Cycles* 30:1692–98
- Groeskamp S, Sloyan BM, Zika JD, McDougall TJ. 2017. Mixing inferred from an ocean climatology and surface fluxes. *J. Phys. Oceanogr.* 47:667–87
- Groeskamp S, Zika JD, McDougall TJ, Sloyan BM, Laliberté F. 2014a. The representation of ocean circulation and variability in thermodynamic coordinates. *J. Phys. Oceanogr.* 44:1735–50



- Groeskamp S, Zika JD, Sloyan BM, McDougall TJ, McIntosh PC. 2014b. A thermohaline inverse method for estimating diathermohaline circulation and mixing. *J. Phys. Oceanogr.* 44:2681–97
- Hautala SL. 2018. The abyssal and deep circulation of the Northeast Pacific Basin. *Prog. Oceanogr.* 160:68–82
- Hieronymus M, Nilsson J, Nylander J. 2014. Water mass transformation in salinity-temperature space. *J. Phys. Oceanogr.* 44:2547–68
- Hirst AC, Jackett DR, McDougall TJ. 1996. The meridional overturning cells of a world ocean model in neutral density coordinates. *J. Phys. Oceanogr.* 26:775–91
- Holzer M, Primeau FW. 2013. Global teleconnections in the oceanic phosphorus cycle: patterns, paths, and timescales. *J. Geophys. Res. Oceans* 118:1775–96
- IOC (Intergov. Oceanogr. Comm.), SCOR (Sci. Comm. Ocean. Res.), IAPSO (Int. Assoc. Phys. Sci. Oceans). 2010. *The International Thermodynamic Equation of Seawater – 2010: Calculation and Use of Thermodynamic Properties*. Man. Guides 56. Paris: UN Educ. Sci. Cult. Organ.
- Isachsen PE, Mauritzen C, Svendsen H. 2007. Dense water formation in the Nordic Seas diagnosed from sea surface buoyancy fluxes. *Deep-Sea Res. I* 54:22–41
- Isachsen PE, Nøst OA. 2012. The air-sea transformation and residual overturning circulation within the Nordic Seas. *J. Mar. Res.* 70:31–68
- Iselin CO. 1939. The influence of vertical and lateral turbulence on the characteristics of the waters at mid-depths. *Eos Trans. AGU* 20:414–17
- Iudicone D, Madec G, Blanke B, Speich S. 2008a. The role of Southern Ocean surface forcings and mixing in the global conveyor. *J. Phys. Oceanogr.* 38:1377–400
- Iudicone D, Madec G, McDougall TJ. 2008b. Water-mass transformations in a neutral density framework and the key role of light penetration. *J. Phys. Oceanogr.* 38:1357–76
- Iudicone D, Rodgers KB, Plancherel Y, Aumont O, Ito T, et al. 2016. The formation of the ocean's anthropogenic carbon reservoir. *Sci. Rep.* 6:35473
- Iudicone D, Rodgers KB, Stendardo I, Aumont O, Madec G, et al. 2011. Water masses as a unifying framework for understanding the Southern Ocean carbon cycle. *Biogeosciences* 8:1031–52
- Iudicone D, Speich S, Madec G, Blanke B. 2008c. The global conveyor belt from a Southern Ocean perspective. *J. Phys. Oceanogr.* 38:1401–25
- Jackett DR, McDougall TJ. 1997. A neutral density variable for the world's oceans. *J. Phys. Oceanogr.* 27:237–63
- Jamous D, Mémery L, Andrié C, Jean-Baptiste P, Merlivat L. 1992. The distribution of helium 3 in the deep western and southern Indian Ocean. *J. Geophys. Res. Oceans* 97:2243–50
- Klocker A, Abernathey R. 2013. Global patterns of mesoscale eddy properties and diffusivities. *J. Phys. Oceanogr.* 44:1030–46
- Klocker A, McDougall TJ. 2010a. Influence of the nonlinear equation of state on global estimates of dianeutral advection and diffusion. *J. Phys. Oceanogr.* 40:1690–709
- Klocker A, McDougall TJ. 2010b. Quantifying the consequences of the ill-defined nature of neutral surfaces. *J. Phys. Oceanogr.* 40:1866–80
- Klocker A, McDougall TJ, Jackett DR. 2009. A new method for forming approximately neutral surfaces. *Ocean Sci.* 5:155–72
- Large WB, McWilliams J, Doney S. 1994. Oceanic vertical mixing: a review and a model with a nonlocal boundary layer parameterization. *Rev. Geophys.* 32:363–403
- Large WB, Nurser AG. 2001. Ocean surface water mass transformation. In *Ocean Circulation and Climate: Observing and Modelling the Global Ocean*, ed. G Siedler, J Church, J Gould, pp. 317–36. Int. Geophys. Ser. Vol. 77. San Diego, CA: Academic
- Large WG, Yeager S. 2009. The global climatology of an interannually varying air-sea flux data set. *Clim. Dyn.* 33:341–64
- Lee MM, Coward ACC, Nurser AJG. 2002. Spurious diapycnal mixing of the deep waters in an eddy-permitting global ocean model. *J. Phys. Oceanogr.* 32:1522–35
- Lewis MR, Carr ME, Feldman GC, Esaias W, McClain C. 1990. Influence of penetrating solar radiation on the heat budget of the equatorial Pacific Ocean. *Nature* 347:543–45
- Lewis MR, Cullen JJ, Platt T. 1983. Phytoplankton and thermal structure in the upper ocean: consequences of nonuniformity in chlorophyll profile. *J. Geophys. Res. Oceans* 88:2565–70



- Lumpkin R, Speer K. 2007. Global ocean meridional overturning. *J. Phys. Oceanogr.* 37:2550–62
- Lupton JE, Craig H. 1981. A major helium-3 source at 15°S on the East Pacific Rise. *Science* 214:13–18
- MacGilchrist GA, Marshall DP, Johnson HL, Lique C, Thomas M. 2017. Characterizing the chaotic nature of ocean ventilation. *J. Geophys. Res. Oceans* 122:7577–94
- Mackay N, Wilson C, Zika J, Holliday NP. 2018. A regional thermohaline inverse method for estimating circulation and mixing in the Arctic and subpolar North Atlantic. *J. Atmos. Ocean. Technol.* In press. <https://doi.org/10.1175/JTECH-D-17-0198.1>
- MacKinnon J, Laurent LS, Garabato AN. 2013. Diapycnal mixing processes in the ocean interior. In *Ocean Circulation and Climate: A 21st Century Perspective*, ed. G Siedler, SM Griffies, J Gould, JA Church, pp. 159–84. Int. Geophys. Ser. Vol. 103. San Diego, CA: Academic. 2nd ed.
- Marsh R. 2000. Recent variability of the North Atlantic thermohaline circulation inferred from surface heat and freshwater fluxes. *J. Clim.* 13:3239–60
- Marsh R, Josey SA, de Nusser AJG, Cuevas BA, Coward AC. 2005. Water mass transformation in the North Atlantic over 1985–2002 simulated in an eddy-permitting model. *Ocean Sci.* 1:127–44
- Marsh R, Nusser AJG, Megann AP, New AL. 2000. Water mass transformation in the Southern Ocean of a global isopycnal coordinate GCM. *J. Phys. Oceanogr.* 30:1013–45
- Marshall JC, Jamous D, Nilsson J. 1999. Reconciling thermodynamic and dynamic methods of computation of water-mass transformation rates. *Deep-Sea Res. I* 46:545–72
- Marshall JC, Shuckburgh E, Jones H, Hill C. 2006. Estimates and implications of surface eddy diffusivity in the Southern Ocean derived from tracer transport. *J. Phys. Oceanogr.* 36:1806–21
- Marshall JC, Williams RG, Nusser AJG. 1993. Inferring the subduction rate and period over the North Atlantic. *J. Phys. Oceanogr.* 23:1315–29
- Maze G, Forget G, Buckley M, Marshall J, Cerovecki I. 2009. Using transformation and formation maps to study the role of air-sea heat fluxes in North Atlantic Eighteen Degree Water formation. *J. Phys. Oceanogr.* 39:1818–35
- McDougall TJ. 1984. The relative roles of diapycnal and isopycnal mixing on subsurface water mass conversion. *J. Phys. Oceanogr.* 14:1577–89
- McDougall TJ. 1987a. Neutral surfaces. *J. Phys. Oceanogr.* 17:1950–64
- McDougall TJ. 1987b. Thermobaricity, cabbeling, and water-mass conversion. *J. Geophys. Res. Oceans* 92:5448–64
- McDougall TJ. 2003. Potential enthalpy: a conservative oceanic variable for evaluating heat content and heat fluxes. *J. Phys. Oceanogr.* 33:945–63
- McDougall TJ, Barker PM. 2011. *Getting started with TEOS-10 and the Gibbs Seawater (GSW) Oceanographic Toolbox*. TEOS-10 Doc., Sci. Comm. Ocean. Res. (SCOR)/Int. Assoc. Phys. Sci. Oceans (IAPSO) Work. Group 127, Int. Counc. Sci., Paris
- McDougall TJ, Church JA. 1986. Pitfalls with the numerical representation of isopycnal diapycnal mixing. *J. Phys. Oceanogr.* 16:196–99
- McDougall TJ, Groeskamp S, Griffies SM. 2014. On geometrical aspects of interior ocean mixing. *J. Phys. Oceanogr.* 44:2164–75
- McDougall TJ, Jackett DR. 1988. On the helical nature of neutral trajectories in the ocean. *Prog. Oceanogr.* 20:153–83
- McDougall TJ, Jackett DR. 2005. The material derivative of neutral density. *J. Mar. Res.* 63:159–85
- McDougall TJ, Jackett DR, Millero FJ, Pawlowicz R, Barker PM. 2012. A global algorithm for estimating Absolute Salinity. *Ocean Sci.* 8:1117–28
- McDougall TJ, McIntosh PC. 2001. The temporal-residual-mean velocity. Part II: isopycnal interpretation and the tracer and momentum equations. *J. Phys. Oceanogr.* 31:1222–46
- McWilliams J. 1998. Oceanic general circulation model. In *Ocean Modeling and Parameterization*, ed. EP Chassignet, J Verron, pp. 1–44. NATO ASI Math. Phys. Sci. Ser. Vol. 516. Dordrecht, Neth.: Kluwer Acad.
- Megann A. 2018. Estimating the numerical diapycnal mixing in an eddy-permitting ocean model. *Ocean Model.* 121:19–33



Review in Advance first posted on  
September 19, 2018. (Changes may  
still occur before final publication.)

- Montgomery RB. 1938. *Circulation in Upper Layers of Southern North Atlantic Deduced with Use of Isentropic Analysis*. Pap. Phys. Oceanogr. Meteorol. Vol. 6. Cambridge, MA/Woods Hole, MA: Mass. Inst. Technol. and Woods Hole Oceanogr. Inst.
- Morel A, Antoine D. 1994. Heating rate within the upper ocean in relation to its bio-optical state. *J. Phys. Oceanogr.* 24:1652–65
- Munk WH. 1966. Abyssal recipes. *Deep-Sea Res. Oceanogr. Abstracts* 13:707–30
- Munk WH, Wunsch C. 1998. Abyssal recipes II: energetics of tidal and wind mixing. *Deep-Sea Res. I* 45:1977–2010
- Nakamura N. 2001. A new look at eddy diffusivity as a mixing diagnostic. *J. Atmos. Sci.* 58:3685–701
- Naveira Garabato AC, Stevens DP, Heywood KJ. 2003. Water mass conversion, fluxes, and mixing in the Scotia Sea diagnosed by an inverse model. *J. Phys. Oceanogr.* 33:2565–87
- Nishikawa S, Tsujino H, Sakamoto K, Nakano H. 2013. Diagnosis of water mass transformation and formation rates in a high-resolution GCM of the North Pacific. *J. Geophys. Res. Oceans* 118:1051–69
- Nurser AJG, Marsh R, Williams RG. 1999. Diagnosing water mass formation from air-sea fluxes and surface mixing. *J. Phys. Oceanogr.* 29:1468–87
- Ohlmann JC. 2003. Ocean radiant heating in climate models. *J. Clim.* 16:1337–51
- Olbers D, Willebrand J, Eden C. 2012. *Ocean Dynamics*. Berlin: Springer
- Pelichero V, Sallée JB, Chapman CC, Downes SM. 2018. The Southern Ocean meridional overturning in the sea-ice sector is driven by freshwater fluxes. *Nat. Commun.* 9:1789
- Pemberton P, Nilsson J, Hieronymus M, Meier HM. 2015. Arctic Ocean water mass transformation in S-T coordinates. *J. Phys. Oceanogr.* 45:1025–50
- Polzin KL, Toole JM, Ledwell JR, Schmitt RW. 1997. Spatial variability of turbulent mixing in the abyssal ocean. *Science* 276:93–96
- Redi MH. 1982. Oceanic isopycnal mixing by coordinate rotation. *J. Phys. Oceanogr.* 12:1154–58
- Richardson PL. 2008. On the history of meridional overturning circulation schematic diagrams. *Prog. Oceanogr.* 76:466–86
- Rumford B. 1968 (1798). Of the propagation of heat in fluids. In *Collected Works of Count Rumford*, Vol. 1: *The Nature of Heat*, ed. SC Brown, pp. 117–284. Cambridge, MA: Belknap
- Sallée JB, Speer K, Rintoul S, Wijffels S. 2010. Southern Ocean thermocline ventilation. *J. Phys. Oceanogr.* 40:509–29
- Sarmiento JL, Gruber N. 2006. *Ocean Biogeochemical Dynamics*. Princeton, NJ: Princeton Univ. Press
- Sarmiento JL, Gruber N, Brzezinski MA, Dunne JP. 2004. High-latitude controls of thermocline nutrients and low latitude biological productivity. *Nature* 427:56–60
- Skliris N, Zika JD, Herold L, Josey SA, Marsh R. 2018. Mediterranean sea water budget long-term trend inferred from salinity observations. *Clim. Dyn.* In press. <https://doi.org/10.1007/s00382-017-4053-7>
- Skliris N, Zika JD, Nurser G, Josey SA, Marsh R. 2016. Global water cycle amplifying at less than the Clausius-Clapeyron rate. *Sci. Rep.* 6:38752
- Sloyan BM, Rintoul SR. 2001. The Southern Ocean limb of the global deep overturning circulation. *J. Phys. Oceanogr.* 31:143–73
- Solomon H. 1971. On the representation of isentropic mixing in ocean circulation models. *J. Phys. Oceanogr.* 1:233–34
- Speer KG. 1993. Conversion among North Atlantic surface water types. *Tellus A* 45:72–79
- Speer KG. 1998. A note on average cross-isopycnal mixing in the North Atlantic Ocean. *Deep-Sea Res. I* 44:1981–90
- Speer KG, Tziperman E. 1992. Rates of water mass formation in the North Atlantic Ocean. *J. Phys. Oceanogr.* 22:93–104
- Sverdrup HU, Johnson MW, Fleming RH. 1942. *The Oceans: Their Physics, Chemistry, and General Biology*. New York: Prentice Hall
- Sweeney C, Gnanadesikan A, Griffies SM, Harrison MJ, Rosati AJ, Samuels BL. 2005. Impacts of shortwave penetration depth on large-scale ocean circulation and heat transport. *J. Phys. Oceanogr.* 35:1103–19
- Talley LD, Yun JY. 2001. The role of cabbeling and double diffusion in setting the density of the North Pacific Intermediate Water salinity minimum. *J. Phys. Oceanogr.* 31:1538–49



- Tamsitt V, Abernathey RP, Mazloff MR, Wang J, Talley LD. 2018. Transformation of deep water masses along Lagrangian upwelling pathways in the Southern Ocean. *J. Geophys. Res. Oceans* 123:1994–2017
- Tandon A, Garrett C. 1997. Water mass formation from thermodynamics: a framework for examining compatibility with dynamics. *International WOCE Newsletter* 28, Oct., pp. 34–37
- Taylor G. 1921. Diffusion by continuous movements. *Proc. Lond. Math. Soc.* 20:196–212
- Toggweiler JR, Samuels B. 1998. On the ocean's large-scale circulation near the limit of no vertical mixing. *J. Phys. Oceanogr.* 28:1832–52
- Treguier AM, Held I, Larichev V. 1997. Parameterization of quasigeostrophic eddies in primitive equation ocean models. *J. Phys. Oceanogr.* 27:567–80
- Urakawa LS, Hasumi H. 2012. Eddy-resolving model estimate of the cabbeling effect on the water mass transformation in the southern ocean. *J. Phys. Oceanogr.* 42:1288–302
- Walin G. 1977. A theoretical framework for the description of estuaries. *Tellus* 29:128–36
- Walin G. 1982. On the relation between sea-surface heat flow and thermal circulation in the ocean. *Tellus* 34:187–95
- Waterhouse AF, MacKinnon JA, Nash JD, Alford MH, Kunze E, et al. 2014. Global patterns of diapycnal mixing from measurements of the turbulent dissipation rate. *J. Phys. Oceanogr.* 44:1854–72
- Whalen CB, Talley LD, MacKinnon JA. 2012. Spatial and temporal variability of global ocean mixing inferred from Argo profiles. *Geophys. Res. Lett.* 39:L18612
- Witte E. 1902. Zur Theorie den Stromkabelungen. *Gaea* 39:229–30
- Worthington LV. 1981. The water masses of the world ocean: some results of a fine-scale census. In *Evolution of Physical Oceanography: Scientific Surveys in Honor of Henry Stommel*, ed. BA Warren, C Wunsch, pp. 42–69. Cambridge, MA: MIT Press
- Wunsch C. 1978. The North Atlantic general circulation west of 50°W determined by inverse methods. *Rev. Geophys.* 16:583–620
- Wüst G. 1936. Das Bodenwasser und die Gliederung der Atlantischen Tiefsee. In *Wissenschaftliche Ergebnisse der Deutschen Atlantischen Expedition auf dem Forschungs- und Vermessungsschiff "Meteor"*, Vol. 6: *Schichtung und Zirkulation des Atlantischen Ozeans*, by G Wüst, A Defant, pp. 3–107. Berlin: Walter de Gruyter
- Zhai P, Rodgers KB, Griffies SM, Slater RD, Iudicone D, et al. 2017. Mechanistic drivers of reemergence of anthropogenic carbon in the equatorial Pacific. *Geophys. Res. Lett.* 44:9433–39
- Zika JD, England MH, Sijp WP. 2012. The ocean circulation in thermohaline coordinates. *J. Phys. Oceanogr.* 42:708–24
- Zika JD, McDougall TJ, Sloyan BM. 2010. Weak mixing in the eastern North Atlantic: an application of the tracer-contour inverse method. *J. Phys. Oceanogr.* 40:1881–93
- Zika JD, Skliris N, Nurser AJG, Josey SA, Mudryk L, et al. 2015. Maintenance and broadening of the ocean's salinity distribution by the water cycle. *J. Clim.* 28:9550–60

